Terminal area control rules and eVTOL adaptive scheduling model for multi-vertiport system in urban air Mobility

城市空中交通终端区域控制规则与多起降点系统中 eVTOL 自适应调度模型

Quan Shao [a,1,*] , Mengxue Shao [a,1] , Yang Lu [b]
邵权 [a,1,*] ，邵梦雪 [a,1] ，卢阳 [b]
[a] College of Civil Aviation, Nanjing University of Aeronautics and Astronautics, Nanjing 211100, China
[a] 南京航空航天大学民航学院，南京 211100，中国
[b] College of Aerospace Engineering, Nanjing University of Aeronautics and Astronautics, Nanjing 211100, China
[b] 南京航空航天大学航空学院，南京 211100，中国

A R T I C L E I N F O

文章信息

Keyword:
关键词:
Urban air mobility
城市空中出行
eVTOL
电动垂直起降飞机 (eVTOL)
Adaptive control system
自适应控制系统
Operational structure
运营结构
Scheduling model
调度模型
Multi-vertiport system
多起降点系统

A B S T R A C T

摘要

On the one hand, vertiports in economically developed areas will present the operation mode of multi-vertiport, and the contradiction between the development of urban air mobility and limited operating resources is very serious. On the other hand, unlike fixed-wing aircraft or helicopters, the electric vertical take-off and landing (eVTOL) aircraft have different operating processes and limited battery energy supply. Long flight times in the terminal area pose a risk of exhaustion and great safety challenges. Given the terminal area of the multi-vertiport system (MVS-TA), this paper investigates the adaptive control system (ACS), which includes the design of the operating environment and the integrated scheduling model. The design of the operating environment is the basis of adaptive management, which consists of the concept of multi-ring structure and the junction control rules based on backpressure policy. Considering the power constraint and dynamic priority, an integrated model including path planning model and distributed sequencing model is constructed to solve the cooperative scheduling problem of approach-departure flights. Results from numerical analyses reveal that: First, in the case of large flight flow, ACS can achieve the efficiency and safety of MVS-TA operation better than the traditional control system. Secondly, the flight density into the terminal area has a greater impact on ACS performance relative to flight volume. With a density of less than 120 flights/hour, the operating efficiency of MVS-TA under ACS varies within 10.3% with the number of flights or density.

一方面，经济发达地区的起降点将呈现多起降点运营模式，城市空中出行的发展与有限的运营资源之间的矛盾非常严重。另一方面，与固定翼飞机或直升机不同，电动垂直起降 (eVTOL) 飞机具有不同的运营流程和有限的电池能量供应。在终端区域长时间飞行存在耗尽的风险和巨大的安全挑战。考虑到多起

降点系统的终端区域 (MVS-TA)，本文研究了自适应控制系统 (ACS)，包括运营环境的设计和集成调度模型的设计。运营环境的设计是自适应管理的基础，包括多环结构的概念和基于背压策略的连接控制规则。考虑到功率约束和动态优先级，构建了一个包括路径规划模型和分布式排序模型的集成模型，以解决进近-起飞航班协同调度问题。数值分析的结果显示: 首先，在大型飞行流量的情况下，ACS 能够比传统控制系统更好地实现 MVS-TA 操作的效率和安全性。其次，与飞行量相比，进入终端区域的飞行密度对 ACS 性能的影响更大。当密度小于 120 架次/小时时，在 ACS 下 MVS-TA 的运营效率随着航班数量或密度的变化而变化，变化范围在 10.3% 。

1. Introduction

1. 引言

1.1. Background

1.1. 背景

The commercial Urban Air Mobility (UAM) operations can be traced back to the United States in the 1840s (Pradeep, 2019). For example, Las Vegas Airlines and New York Airlines are used to transport people and mail between several locations. Although the operation of UAM was gradually terminated in the 1880s (Pradeep, 2019) due to accidents caused by mechanical failure, there is still a demand for commercial UAM operations to avoid transportation congestion on the ground.

商业化的城市空中出行 (UAM) 业务可以追溯到 19 世纪 40 年代的美国 (Pradeep，2019)。例如，拉斯维加斯航空公司和纽约航空公司曾被用来在多个地点之间运送人员和邮件。尽管由于机械故障导致的事故，UAM 的业务在 19 世纪 80 年代逐渐停止 (Pradeep，2019)，但仍然存在对商业 UAM 业务的需求，以避免地面交通拥堵。

However, current aviation technologies have reached a level of maturity to enable UAM to use quiet and efficient vehicles to conduct on-demand and scheduled operations (Thipphavong et al., 2018). UAM is a new type of urban low-altitude transportation application, which uses a small all-electric or hybrid-electric vertical take-off and landing vehicle (VTOL) as the main means of transport to provide sustainable and affordable passenger or cargo transport services (Li et al., 2020; Thipphavong et al., 2018). Electric Vertical Take-Off and Landing (eVTOL) aircraft integrates advanced autonomous flight and distributed power technology. Complementing the traditional rotorcraft with longer voyages, eVTOL will be mainly used for short-air transportation services in urban areas. Its potential markets include, but are not limited to, passenger transportation services (such as air taxis, shuttle services), cargo services (German et al., 2018), medical rescue, public safety (Thipphavong et al., 2018), etc.

然而，当前的航空技术已经成熟到能够使 UAM 使用安静且高效的交通工具进行按需和计划内的运营 (Thipphavong 等，2018)。UAM 是一种新型的城市低空交通应用，它使用小型全电动或混合电动垂直起降飞机 (VTOL) 作为主要运输方式, 提供可持续且负担得起的乘客或货物运输服务 (Li 等, 2020; Thipphavong 等，2018)。电动垂直起降 (eVTOL) 飞机集成了先进的自主飞行和分布式动力技术。与传统旋翼飞机相比，eVTOL 具有更长的航程，主要用于城市区域的短途空中运输服务。其潜在市场包括但不限于乘客运输服务 (如空中出租车、穿梭服务)、货运服务 (German 等，2018)、医疗救援、公共安全 (Thipphavong 等，2018) 等。

The key issues in the development of UAM include automated flight and contingency management, airspace system design, community integration, distributed power systems, reliability, etc. (Littell, 2019; Thipphavong et al., 2018; Vascik and Hansman, 2018). From the point of view of airspace structure design and operation management, this paper studies the efficient operation of the UAM terminal area. Due to UAM's mission positioning and application needs, the economically developed and densely populated metropolitan area will certainly have the trend of vertiport-intensive distribution, two or more vertiports in a certain area of cooperation, involving the sharing and competition of space-time resources between multiple vertiports, that is, the "Multi-vertiport System (MVS)" development mode. The operation control problem of the MVS-TA is one of the important links in the airspace management system, which focuses on how to design the route structure, operating rules, and control

* Corresponding authors.
* 通讯作者。
E-mail address: shaoquan@nuaa.edu.cn (Q. Shao).
电子邮件地址:shaoquan@nuaa.edu.cn(Q. Shao)。
[1] Quan Shao and Mengxue Shao are co-first authors of the article.
[1] Quan Shao 和 Mengxue Shao 是本文的共同第一作者。

strategy to adapt to the operation characteristics of high density and high traffic in the terminal area and the power limit of eVTOL.

无人航空交通 (UAM) 发展的关键问题包括自动化飞行和应急管理等，空域系统设计、社区整合、分布式动力系统、可靠性等 (Littell, 2019; Thipphavong et al., 2018; Vascik and Hansman, 2018)。从空域结构设计与运营管理的角度来看，本文研究了 UAM 终端区的有效运行。由于 UAM 的使命定位和应用需求，经济发达且人口密集的都市区将肯定出现垂直机场密集分布的趋势，某一区域内两个或更多的垂直机场进行合作，涉及多个垂直机场之间的时空资源共享与竞争，即“多垂直机场系统 (MVS)”发展模式。MVS-TA 的运行控制问题是空域管理系统中的关键环节，重点关注如何设计航线结构、运行规则和控制策略，以适应终端区高密度和高交通流的运行特性以及 eVTOL 的功率限制。

The existing air traffic management means are relatively ineffective. First of all, eVTOL has different operational processes and limited power, and the types of aircraft targeted by traditional civil aviation or general aviation air traffic control methods are completely different. Inefficient and cumbersome scheduling can cause flights to delay too long, creating the risk of running out of power and great safety challenges. Second, UAM's main operating airspace is concentrated in Class E, Class G airspace, or low airspace below 1000 m (inclusive) (Thipphavong et al.,2018). High-density traffic environments, urban airspace environments, and conflict resolution can greatly increase the complexity of scheduling strategies. The traditional scheduling method is based on flight planning or deterministic operating environment, obviously cannot effectively solve the MVS-TA flight scheduling problem. Even the UAS Traffic Management Framework (UTM) being built by countries (Prevot et al., 2016) is only for small unmanned aerial vehicles in airspace below 120 m , which can neither cover the airspace of UAM nor fully meet the management needs of MVS (Mohamed Salleh et al., 2017).

现有的空中交通管理手段相对低效。首先，eVTOL 具有不同的运营流程和有限的动力，传统民用航空或通用航空空中交通管制方法针对的飞机类型与之完全不同。低效且繁琐的调度可能导致航班延误过长，从而产生耗尽动力和巨大的安全挑战。其次，UAM 的主要运营空域集中在 E 类、G 类空域，或 1000 m (含) 以下的低空 (Thipphavong 等人，2018 年)。高密度交通环境、城市空域环境和冲突解决大大增加了调度策略的复杂性。传统的调度方法基于航班规划或确定性运行环境，显然无法有效解决 MVS-TA 航班调度问题。即便是各国正在构建的无人机交通管理框架 (UTM)(Prevot 等人，2016 年) 也仅适用于 120 m 以下的空域中的小型无人机，无法覆盖 UAM 的空域，也无法完全满足 MVS 的管理需求 (Mohamed Salleh 等人，2017 年)。

1.2. Literature review

1.2. 文献综述

The study of airspace structure in the UAM terminal area is usually combined with flight scheduling. (Bertram and Wei, 2020) proposes an airspace design of a terminal area containing boundaries and several centric rings. Markov Decision Model (MDP) is used to schedule flights around the ring layer. use the to guide the operation of flights. (Kleinbekman et al., 2018) initially designed the route structure with multiple arrival fixes/routes. Drawing on the concept of dynamic geofencing in UTM, (Zhu and Wei, 2019) proposes a conflict-free route pre-planning method to achieve on-demand occupancy of airspace, based on which a pre-planning algorithm for departure flight trajectories based on two-stage optimization is constructed.

对 UAM 终端区空域结构的研究通常与航班调度相结合。(Bertram 和 Wei，2020 年) 提出了一个包含边界和几个中心环的终端区域空域设计。使用马尔可夫决策模型 (MDP) 对环形层周围的航班进行调度。使用该方法来指导航班运行。(Kleinbekman 等人，2018 年) 最初设计了具有多个到达定位点/航线的航线结构。借鉴 UTM 中的动态地理围栏概念，(Zhu 和 Wei，2019 年) 提出了一种无冲突航线预规划方法，以实现按需占用空域，基于此构建了一个基于两阶段优化的出发航班轨迹预规划算法。

In terms of urban airspace route structure design, the Metroplis team proposed the concept of unstructured airspace (Full Mix) operation and three types of structured airspace (Layers, Zones, Tubes). Comparing the four urban airspace structures from the perspectives of traffic density, complexity, and robustness, (Vidosavljevic et al., 2015) considered that Layers have a good balance between completely unstructured concepts and structured concepts, which is the best concept of complexity. Since there are many conflicts and intrusions in each concept, (Sunil et al., 2016) recommends investigating novel conflict detection and resolution algorithms that cope with the limited maneuvering room available at extreme traffic densities. To meet eVTOL's need for dynamic changes in urban airspace, (Mohammed Salleh et al., 2018) has planned three route structures for UAM: route network in AirMatrix, route network over buildings, and route network over Roads, and evaluates the performance in terms of capacity and throughput. The AirMatrix-based route can meet the needs of larger airspace capacity and traffic throughput, but it requires a highly automated and robust UAM management system for unified scheduling.

在城市空域路由结构设计方面，Metroplis 团队提出了无结构空域 (Full Mix) 操作的概念以及三种结构

化空域类型 (层级、区域、管道)。从交通密度、复杂性和鲁棒性角度比较四种城市空域结构，(Vidosavljevic 等人，2015 年) 认为层级概念在完全无结构概念和结构化概念之间取得了良好的平衡，是最佳复杂度概念。由于每个概念中存在许多冲突和入侵，(Sunil 等人，2016 年) 建议研究新型冲突检测和解决算法，以应对极端交通密度下的有限机动空间。为了满足 eVTOL 在城市空域中动态变化的需求，(Mohammed Salleh 等人，2018 年) 为 UAM 规划了三种路由结构: 基于 AirMatrix 的路由网络、建筑上方的路由网络和道路上方路由网络，并从容量和吞吐量方面评估性能。基于 AirMatrix 的路由可以满足更大空域容量和交通吞吐量的需求，但它需要一个高度自动化和鲁棒的 UAM 管理系统来进行统一调度。

For on-demand features of UAM flights, (Pradeep, 2019) proposes the concept of Required Times of Arrival (RTA) to schedule approach flights. The study used Mixed-integer Linear Programming (MILP) models and Time-advance (TA) strategies to schedule RTAs for flights to reduce their air waiting times in the terminal area. Further to the approach process, (Pradeep, 2019) and (Pradeep and Wei, 2018) put forward the method of absorbing delay by optimizing speed and Shallow Descent flight, respectively, to obtain the energy-saving trajectory with the assigned RTA. Based on MILP and shallow descent control, the approach sequence satisfying RTA is calculated under the limits of residual battery power and vertiport capacity, but the system can only effectively handle the scheduling of 40 flights at most at frequency of 40 arrivals/hr (Kleinbekman et al., 2018). Expanding the research problem to the double-vertipad vertiport, (Kleinbekman et al., 2020) builds a rolling-horizon scheduling model that optimizes the average delay time of eVTOL to 50 s of the RTA. Besides, (Brittain and Wei, 2018)applied a hierarchical deep reinforcement learning framework to the sequencing and interval management of approaching flights. However, the robustness of artificial intelligence methods applied to air traffic management needs to be further improved.

针对 UAM 航班按需特性的需求，(Pradeep，2019) 提出了所需到达时间 (RTA) 的概念来安排进近航班。该研究使用了混合整数线性规划 (MILP) 模型和时间提前 (TA) 策略来为航班安排 RTA，以减少其在终端区域的空中等待时间。在进近过程之后，(Pradeep，2019) 和 (Pradeep 和 Wei，2018) 分别提出了通过优化速度和浅降飞行来吸收延迟的方法，以获得指定 RTA 的节能轨迹。基于 MILP 和浅降控制，计算满足 RTA 的进近序列，受到剩余电池电量和垂直机场容量的限制，但系统最多只能有效处理频率为每小时 40 个到达的 40 个航班的调度 (Kleinbekman 等人，2018)。将研究问题扩展到双起降点的垂直机场，(Kleinbekman 等人，2020) 构建了一个滚动时间窗口调度模型，将 eVTOL 的平均延迟时间优化为 RTA 的 50 秒。此外，(Brittain 和 Wei，2018) 将分层深度强化学习框架应用于进近航班的排序和间隔管理。然而，应用于空中交通管理的人工智能方法的鲁棒性需要进一步改进。

In the control of UAM operation process, (Bosson and Lauderdale, 2018) presents an initial implementation of autonomous network management and aircraft separation service, and analyzes the impact of space interval, time interval and arrival scheduling horizon on delay time and conflict resolution. To achieve eVTOL conflict-avoidance and autonomous flight, the methods used at present include Markov Decision Model (MDP) (Bertram and Wei, 2020; Yang et al., 2019), autonomous network management and separation services (Bosson and Lauderdale, 2018), pre-flight planning based on dynamic geofence(Zhu and Wei, 2019), etc.

在 Urban Air Mobility(UAM) 运营过程的控制中，(Bosson 和 Lauderdale，2018) 提出了自主网络管理和飞机分离服务的初步实施，并分析了空间间隔、时间间隔和到达调度时间范围对延迟时间和冲突解决的影响。为了实现 eVTOL 避障和自主飞行，目前使用的方法包括马尔可夫决策模型 (MDP)(Bertram 和 Wei，2020；Yang 等人，2019)，自主网络管理和分离服务 (Bosson 和 Lauderdale，2018)，基于动态地理围栏的飞行前规划 (Zhu 和 Wei，2019) 等。

Overall, the multi-faceted study of UAM terminal area is of great reference significance, but there are still the following problems 1) The study of the airspace structure of the terminal area is usually limited to the concept of simple route structure, which is difficult to cope with the operation of UAM high-traffic high-density flights, and cannot improve the efficiency of flight operation from the mechanism. 2) The flight scheduling in the terminal area is limited to the optimization of approach or departure of a single, and the process of approach and departure is completely stripped off. MVS has the characteristics of many components, complex airspace structure and large flight flow, not a simple composite of a single vertiport. Existing research cannot achieve MVS resource coordination and integrated optimization. 3) At this stage, the conflict avoidance study is not combined with the design of the airspace structure of the terminal area. In the mature stage of UAM, which is complex in airspace network and requires fine and flexible management, it is difficult to guarantee the system efficiency and safety level.

总的来说，对 UAM 终端区域的多方面研究具有很大的参考意义，但仍然存在以下问题:1) 对终端区域空域结构的研究通常仅限于简单路由结构的概念，这难以应对 UAM 高流量高密度航班的运营，也无法从机制上提高飞行运营的效率。2) 终端区域的飞行调度仅限于对单个进近或离港的优化，进近和离港的过程被完全剥离。MVS 具有组件多、空域结构复杂、航班流量大的特点，不是单个垂直起降场的简单组合。现有研究无法实现 MVS 资源的协调和一体化优化。3) 目前，避障研究没有与终端区域空域结构的设计相结合。在 UAM 成熟阶段，空域网络复杂且需要精细灵活的管理，很难保证系统的效率和安全性水平。

The flight sorting and dispatching method of the regional multi-airport terminal area in the traditional civil aviation field is used as the baseline. This paper designs a complete MVS-TA adaptive management system in-

cluding route structure, control rules and scheduling optimization, which aims to improve the operation efficiency of MVS-TA in medium-high density areas at an acceptable safety level. The contributions of this paper include three aspects: 1) In view of the characteristics of the dense distribution of ver-tiports, the concept of MVS and the structure design of multi-ring are put forward. 2) By adding the road capacity constraints into the backpressure strategy, a model of the intersection control rules of MVS-TA is constructed 3) The integrated adaptive scheduling model, which includes the dynamic time-saving path planning model and the sequencing model at the transit junction, is proposed to realize the coordinated scheduling of approach-departure flights and distributed control.

本文以传统民航领域区域多机场终端区的航班排序和调度方法作为基准。设计了一套完整的 MVS-TA 自适应管理系统，包括航线结构、控制规则和调度优化，旨在在可接受的安全水平上提高中等至高密度区域 MVS-TA 的运行效率。本文的贡献包括三个方面:1) 鉴于垂起机场密集分布的特点，提出了 MVS 概念和多环结构设计。2) 通过将道路容量约束纳入背压策略，构建了 MVS-TA 交叉控制规则模型。3) 提出了包含动态节时路径规划模型和换乘节点排序模型的综合自适应调度模型，以实现进离场航班的协同调度和分布式控制。

The rest of this paper is organized as follows: Section II designed the multi-ring operation structure for the MVS terminal area, and constructed the control rules of junctions based on the cyclic phase backpressure strategy. Based on traffic structure and operation control rules, Section III constructs the integrated adaptive scheduling model for MVS. Section IV combs the implementation framework and algorithm flow of the ACS. Example simulation and result analysis are described in section V. Section VI concludes the paper.

本文其余部分安排如下: 第二节设计了 MVS 终端区的多环运行结构，并基于循环相背压策略构建了交叉控制规则。基于流量结构和运行控制规则，第三节构建了 MVS 的综合自适应调度模型。第四节梳理了 ACS 的实施框架和算法流程。第五节描述了示例仿真和结果分析。第六节对本文进行了总结。

2.The conceptual structure and operating rules of the multi-vertiport system

2. 多垂起机场系统的概念结构和运行规则

According to the operation characteristics and the flight process of eVTOL, this section designs a route structure including multiple rings and transit junctions for the Terminal Area of Multi-vertiport system (MVS-TA), which is the main innovation of this chapter. Further, the backpressure control strategy is introduced into UAM's intersection control and segment capacity constraints are added to make it more applicable.

根据 eVTOL 的运行特性和飞行流程，本节为多垂起机场系统终端区 (MVS-TA) 设计了一个包括多环和中转节点的航线结构，这是本章的主要创新。进一步地，将背压控制策略引入 UAM 的交叉控制，并增加了段容量约束，使其更具适用性。

A vertiport has one or more vertical take-off and landing platforms (vertipads). The conceptual structure and operation rules of MVS-TA described in this section focus on the terminal area and do not involve the scheduling rules between the vertipads of each vertiport. Moreover, the conceptual structure and operating rules described in this section are also applicable to the terminal area of a single vertiport with multiple vertipads. Without considering the optimal scheduling between vertipads, the integrated adaptive scheduling model (section 3) is also applicable.

垂直机场有一个或多个垂直起降平台 (起降坪)。本节中描述的 MVS-TA 的概念结构和操作规则侧重于终端区域，并不涉及每个垂直机场起降坪之间的调度规则。此外，本节中描述的概念结构和操作规则也适用于具有多个起降坪的单个垂直机场的终端区域。在不考虑起降坪之间最优调度的情况下，综合自适应调度模型 (第 3 节) 同样适用。

2.1.The conceptual structure and system modeling of MVS-TA

2.1.MVS-TA 的概念结构和系统建模

2.1.1.The conceptual structure of MVS-TA

2.1.1.MVS-TA 的概念结构

The current growth in commercial air traffic has outpaced the capabilities of people-centered systems, and this is only for manned flights. The growth of unmanned and autonomous aircraft will increase traffic by several orders of magnitude. NASA predicts that as UAM reaches maturity (UML-5), a city will accommodate more than 1,000

eVTOL aircraft in a typical 30 to 40n mile diameter range, with airspace density 400 times the allowable IFR density (Mueller, 2019). Constraints on air traffic control workload are a key factor limiting the speed and density of UAM operations. Developing concepts, techniques, and procedures for UAM to manage without air traffic control tactical intervention, and implementing rule-based information communication of system elements, is an important part of achieving higher density, faster-paced UAM operation (Thipphavong et al., 2018). Therefore, this paper starts from the route structure and operating rules of MVS-TA to ensure the safe and efficient operation of medium-high density approach-departure flights in complex airspace.

当前商业航空交通的增长速度已经超过了以人为中心的系统的处理能力，这仅针对有人驾驶航班。无人和自主飞行器的增长将使交通量增加几个数量级。NASA 预测，随着城市空中交通 (UAM) 成熟 (UML-5)，一个城市将在典型的 30 至 40 海里直径范围内容纳超过 1000 架 eVTOL 飞行器，空域密度是允许的仪表飞行规则 (IFR) 密度的 400 倍 (Mueller, 2019)。空中交通管制工作量的限制是限制 UAM 运行速度和密度的一个关键因素。开发 UAM 管理概念、技术和程序，无需空中交通管制战术干预，并实施基于规则的系统元素信息通信，是实现更高密度、更快节奏 UAM 运行的重要部分 (Thipphavong 等人，2018 年)。因此，本文从 MVS-TA 的航线结构和操作规则出发，确保在复杂空域中中等至高密度进近-起飞航班的安全和高效运行。

The operation schedule of the flights is based on a new generation of CNS (communication, navigation, and surveillance) networks (e.g. VHF OMF VOR, WIDE Enhancement System, etc.) and high-capacity, low-latency precision guidance for navigation equipment (Thipphavong et al., 2018). Each eVTOL is the subject of the CNS network. Ground base stations can collect real-time data and transmit information to each aircraft during operation. Each aircraft can also clarify the location information of other flight subjects (including traditional flights) within a certain range while receiving the ground base station dispatch instructions. The system's CNS network and data transmission are particularly important in areas with low visibility, large buildings, and densely populated areas.

航班的运行计划是基于新一代的 CNS(通信、导航和监视) 网络 (例如 VHF OMF VOR、WIDE 增强系统等) 以及高容量、低延迟的精密导航设备指导 (Thipphavong 等人，2018 年)。每一架 eVTOL 都是 CNS 网络的主体。地面基站能够收集实时数据并在运行期间向每架飞机传输信息。每架飞机在接收到地面基站调度指令的同时，也能明确一定范围内其他飞行主体 (包括传统航班) 的位置信息。在能见度低、建筑物高大、人口密集的地区，系统的 CNS 网络和数据传输尤为重要。

Specifically, the MVS-TA designed in this paper is a radiant structure (Fig. 1) including the approach-departure rings, emergency ring, junctions, approach-departure routes, and waiting areas (holding stack). The ring layers are concentric circles with different radius and heights, which form the "frustum of a cone" shape (Fig. 2), to accommodate the operating characteristics of frequent altitude changes as the aircraft enters/leaves the terminal area. The vertical take-off and landing point is 200 m away from the ver-tiport, which is the transition point between the vertical flight and the approach-departure program. The system consists of several vertiports $V = \{V_1, V_2, \cdots, V_N\}$ and approach-departure rings. The outermost ring layer (Starting ring layer Ring_A) is the boundary between the terminal area and other airspaces. The middle ring layer and the final ring layer are used for route planning and scheduling of flights. They are divided into two parts by the line passing through the diameter of the concentric circle: the approach ring layer (Middle approach layer Ring_{A-B} , Final approach layer Ring_{A-C}) and departure ring layer (Middle departure layer Ring_{D-B} , Final departure layer Ring_{D-C}). The approach side and the departure side switch in different directions but connected, the aircraft can operate around the ring layer. Each ring level includes several transit junctions.

具体来说，本文设计的 MVS-TA 是一种辐射结构 (图 1)，包括进离场环、紧急环、连接点、进离场路线和等待区域 (等待栈)。环层是由不同半径和高度的同心圆组成，形成“圆锥台”形状 (图 2)，以适应飞机进入/离开终端区域时频繁的高度变化操作特性。垂直起降点距离机场 200 m 处，是垂直飞行与进离场程序的转换点。系统由几个机场 $V = \{V_1, V_2, \cdots, V_N\}$ 和进离场环组成。最外层的环层 (起始环层 Ring_A) 是终端区域与其他空域的边界。中间环层和最终环层用于航路规划和航班调度。它们通过同心圆直径的直线分为两部分: 进场环层 (中间进近层 Ring_{A-B} 、最终进近层 Ring_{A-C}) 和离场环层 (中间离场层 Ring_{D-B} 、最终离场层 Ring_{D-C})。进场侧和离场侧在不同方向上切换但相互连接，飞机可以在环层周围运行。每个环层级包括几个过渡连接点。

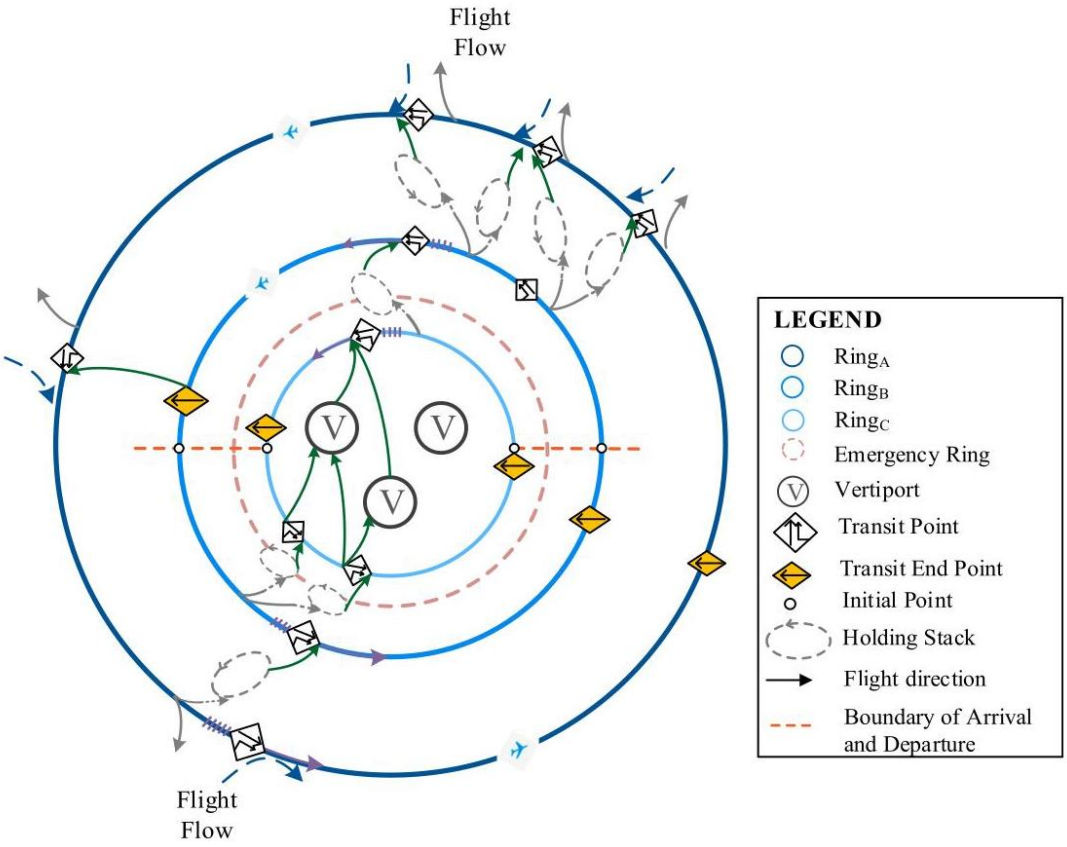

Fig. 1. Operational concept design for terminal airspace of MVS-TA.

图 1。MVS-TA 终端空域的操作概念设计。

Relatively speaking, each transit junction is an important node for frequent changes of aircraft altitude and speed and is an area with a higher risk of dangerous approach. The location planning should not only take into account the airspace structure and the ground base station, but also control and reduce the impact of the operation on the ground buildings and personnel from a safety perspective. This aspect is not within the scope of this article.

相对而言，每个过渡连接点是飞机高度和速度频繁变化的重要节点，也是危险接近风险较高的区域。位置规划应考虑空域结构和地面基站，同时从安全角度控制和减少对地面建筑和人员的影响。这方面的内容不在本文讨论范围内。

Transit junctions can control and dispatch the flow based on the traffic signal issued by the ground base station. According to the difference of control mode, the junctions can be divided into three categories: initial transit junction, composite junction, and transit endpoint. 1) The initial transit junction is the initial node of the switching ring layer (Fig. 4e). 2) The composite intersection structure includes shadow nodes and signal-controlled points. In order to reduce the control load and the risk conflict at the junction, the flight

传输节点可以根据地面基站发出的交通信号控制和调度流量。根据控制方式的不同，节点可以分为三类: 初始传输节点、复合节点和传输端点。1) 初始传输节点是切换环层的初始节点 (图 4e)。2) 复合交叉结构包括阴影节点和信号控制点。为了降低节点的控制负载和冲突风险，飞行

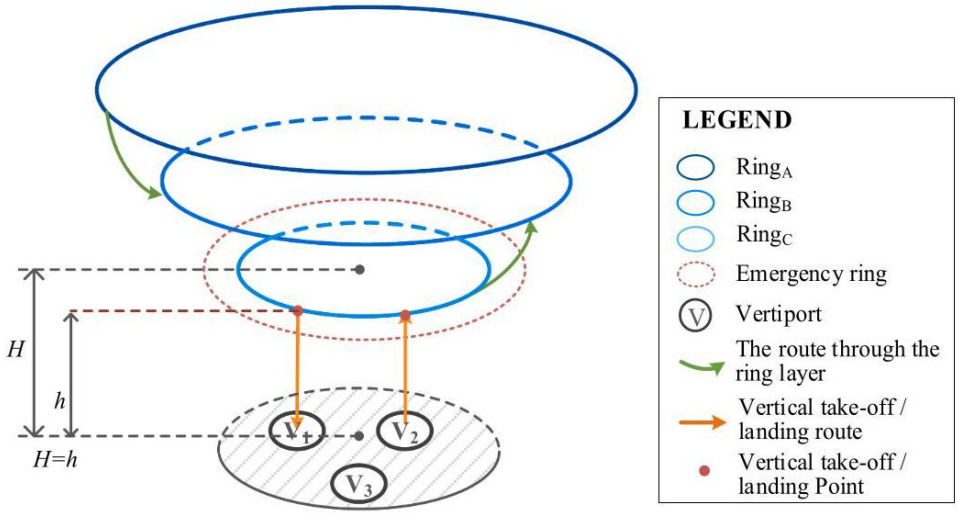

Fig. 2. Three-dimensional diagram of operational concept for MVS-TA.
图 2. MVS-TA 操作概念的三维图。

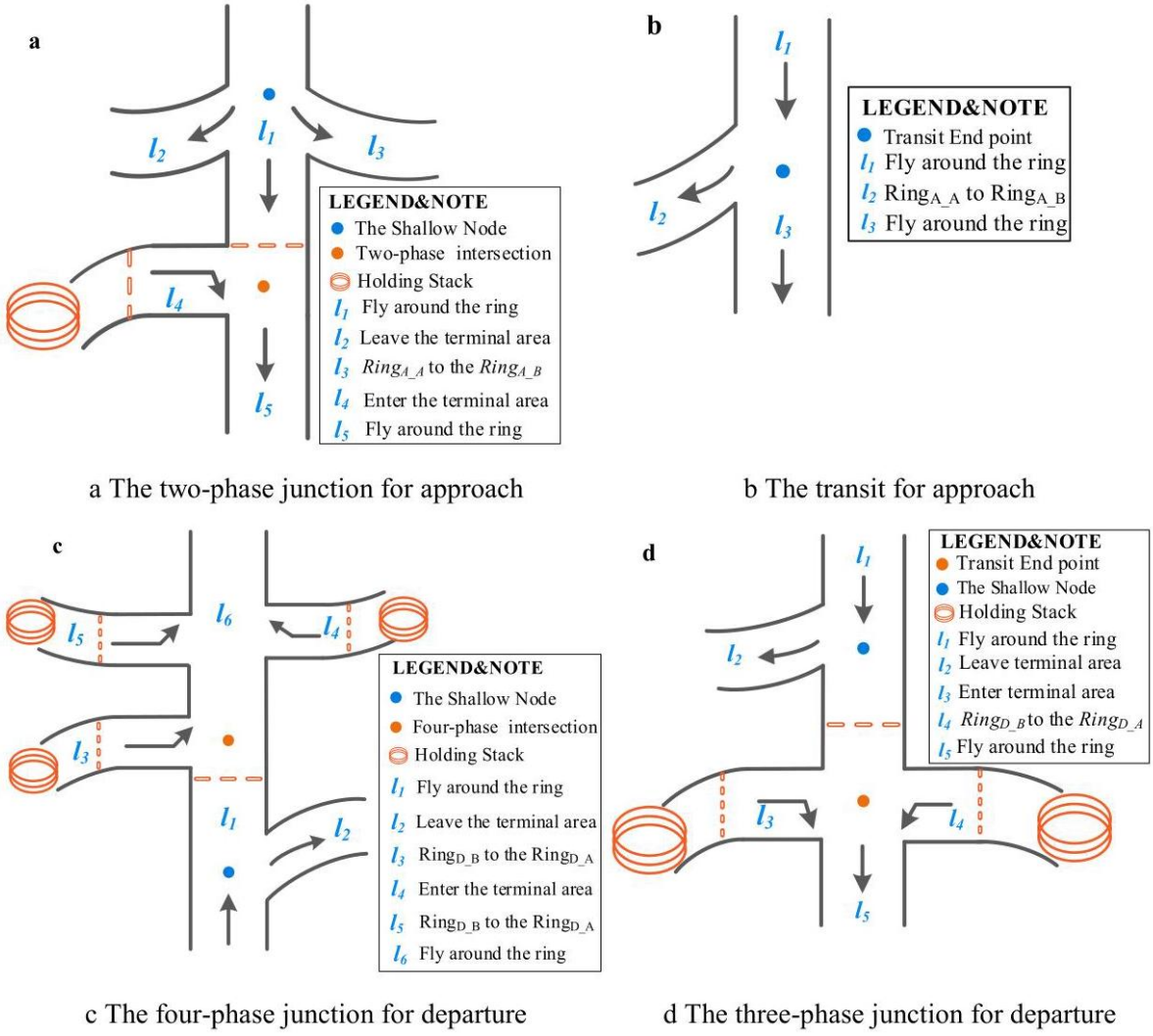

a The two-phase junction for approach

b The transit for approach

c The four-phase junction for departure

d The three-phase junction for departure

Fig. 3. The intersection structure of.Ring $_A$
图 3. 环 $_A$ 的交叉结构。

flow can only sink out of the ring layer at the ”shadow node” in front of the multi-phase transit junction, which is not controlled by the signal light. Flights are only allowed to around or sink into the ring layer in accordance with signal control at each multi-phase transit junction (Fig. 3). 3) The shadow node before the transit endpoint is the last chance for the flight flow in the ring to switch to the inner ring layer. Due to the functional differences of each ring layer in the system, the characteristics of the transit junctions between the different height ring layers and between the approach-departure ring layers are slightly different. Ring$_A$ contains only multi-phase transit junctions and control endpoints (Fig. 3), where approach-departure flights make flight orientation adjustments. Ring $_B$ and Ring$_C$ contain three types of transit junctions (Fig. 4), which realize the adaptive scheduling and improve the operational efficiency through signal control and sequencing optimization of each junction.

流量只能从环层前方多相传输节点前的“阴影节点”中流出，该节点不受信号灯控制。只有在每个多相传输节点根据信号控制进行飞行，才允许飞行围绕或进入环层 (图 3)。3) 在传输端点前的阴影节点是环内飞行流切换到内环层的最后机会。由于系统中每个环层的功能差异，不同高度环层之间以及进近-起飞环层之间的传输节点特性略有不同。Ring$_A$ 仅包含多相传输节点和控制端点 (图 3)，其中进近-起飞飞行进行飞行方向调整。环 $_B$ 和 Ring$_C$ 包含三种类型的传输节点 (图 4)，通过信号控制和每个节点的排序优化实现自适应调度，提高运营效率。

The characteristics of MVS-TA system are summarized as follows: 1) The structure consists of three approach-departure ring layers and one emergency ring layer, which are applied to normal operation and emergency respectively. Flights in emergency situations can operate on the emergency ring, greatly reducing the impact on normal operations of other flights. 2) The operation control of the intersection can greatly reduce the flight conflict from the mechanism. 3) The radiant structure can improve the capacity, operational efficiency, and utilization of airspace resources in the terminal area. The ”frustum of a cone” shape is more suitable for the eVTOL operation. 4) Due to the competition in time and space resources (such as air routes and intersections, etc.), there is competition between vertiports.

MVS-TA 系统的特点可概括如下:1) 结构由三个进近-起飞环形层和一个紧急环形层组成，分别应用于正常操作和紧急情况。紧急情况下的航班可以在紧急环道上运行，大大减少了对其他航班正常运营的影响。2) 交叉操作控制可以大大减少来自机制的航班冲突。3) 辐射结构可以提高终端区域空域资源的容量、运营效率和利用率。圆锥台形状更适合 eVTOL 运行。4) 由于时间资源和空间资源 (如航线和交叉点等) 的竞争，垂直机场之间存在竞争。

2.1.2.A modeled description of the transit junctions of MVS-TA

2.1.2.A MVS-TA 的交汇处建模描述

The traffic network in the MVS-TA can be modeled as a forward figure G containing M transit junctions. The set of transit junctions includes several junctions, which can be expressed as $J = \{j_1, j_2, \cdots, j_M\}$. Each junction j_i includes three parts L_i 、 F_i 、 P_i , representing the set of links, the set of aircraft traffic flows, the set of phases. The link collection $L_i = \left\{l_i^1, l_i^2, \cdots, l_i^N\right\}$, can be divided into two subsets: the set of input links $L_{in}\left(j_i\right)$ and the set of output links $L_{out}\left(j_i\right)$.

MVS-TA 中的交通网络可以被建模为一个前向图 G 包含 M 交汇处。交汇处集合包括几个交汇点，可以表示为 $J = \{j_1, j_2, \cdots, j_M\}$ 。每个交汇点 j_i 包括三部分 L_i 、 F_i 、 P_i ，分别表示链接集合、飞机流量集合、阶段集合。链接集合 $L_i = \left\{l_i^1, l_i^2, \cdots, l_i^N\right\}$ 可以分为两个子集: 输入链接集合 $L_{in}\left(j_i\right)$ 和输出链接集合 $L_{out}\left(j_i\right)$ 。

Suppose the two-phase intersection represented by Fig. 3a is defined as $j_1.l_1^1$ and l_1^4 are both input links, and l_1^5 is the output link, i.e.

假设图 3a 所示的两位相交点定义为 $j_1.l_1^1$ 和 l_1^4 都是输入链接，而 l_1^5 是输出链接，即

$$L_{\text{in}}\left(j_1\right) = \left\{l_1^1, l_1^4\right\} \tag{1}$$

$$L_{\text{out}}\left(j_1\right) = \left\{l_1^5\right\} \tag{2}$$

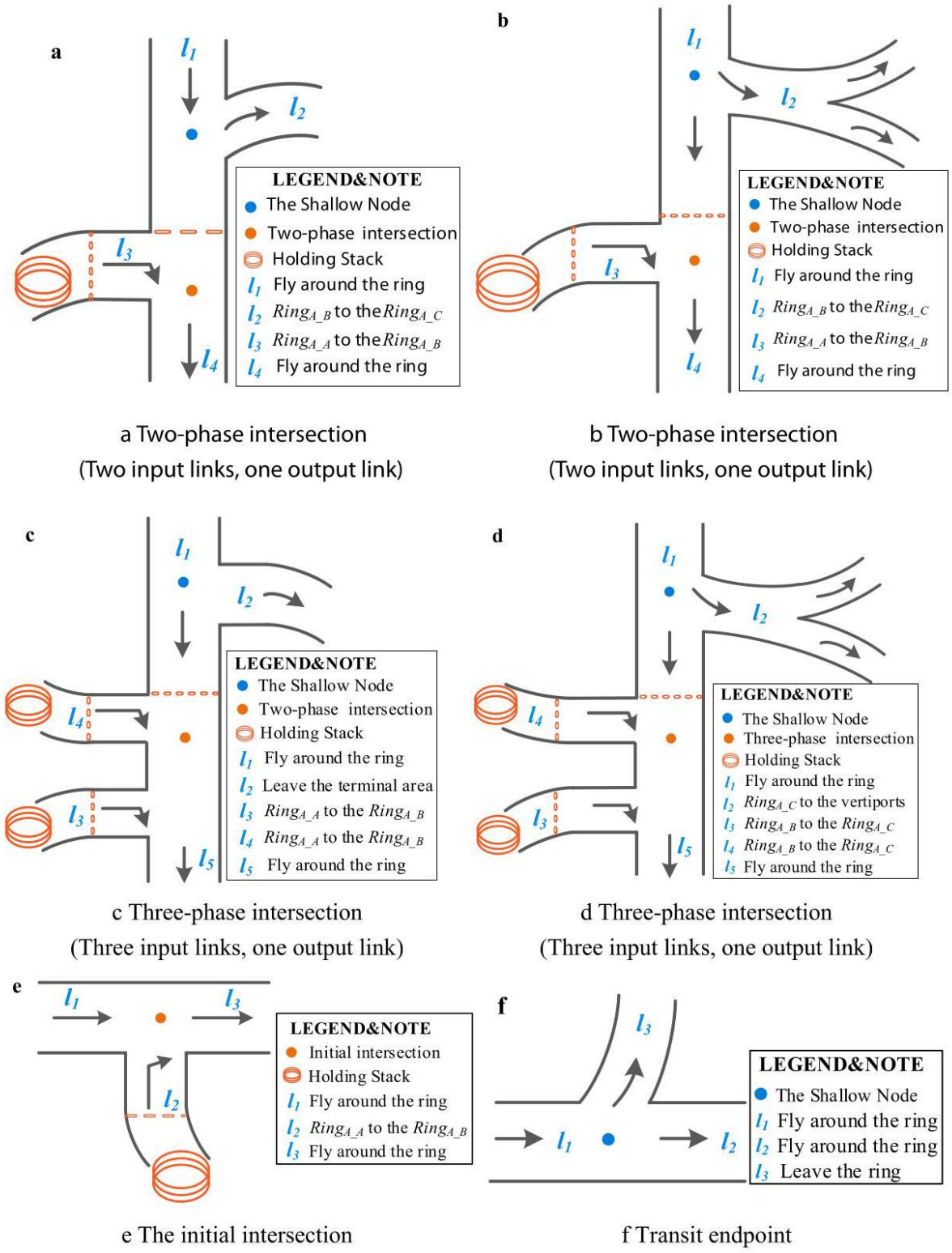

Fig. 4. The intersection structure of the approach side ring layer Ring_{A-B} (Ring_{A-C}) (Note: The junctions of Ring_{D-B} and Ring_{D-C} on the departure side are similar to the approach side. Fig. 4a-Fig. 4d are composite junctions with different multi-phase junction).

图 4. 接近侧环层 Ring_{A-B} (Ring_{A-C}) 的交叉结构 (注: 出发侧的 Ring_{D-B} 和 Ring_{D-C} 的接合处与接近侧相似。图 4a-图 4d 是具有不同多相位接合的复合接合)。

The process of aircraft passing through each junction can be regarded as a traffic movement process. When two adjacent links have a feasible path, traffic flows can be transferred from the upstream link to the downstream link. The transfer rate is equal to the saturated rate when the upstream link is oversaturated and is considered 0 when

there are no channels between the two adjacent links. Therefore, when the upstream is oversaturated, the number of aircraft transferred through the corresponding channel is a product of the green light time and saturation flow rate (flight interval is considered). For the flight process collection FD_i of the junction j_i , there is $fd_i^{ab} \in FD_i$, where fd_i^{ab} is the traffic flow from the input link l_i^a to the output link $l_i^b, l_i^a \in L_{in}(j_i), l_i^b \in L_{out}(j_i)$. There is a variety of traffic flow transfer processes at each junction, $L_{in}(j_i) \times L_{out}(j_i)$, which are controlled by different phases to give them access. p_i^k represents the kth phase of the transit junction j_i, P_i is a collection of all phases of junction j_i .

飞机通过每个接合点的过程可以被视为一个交通流动过程。当两个相邻连接之间存在可行路径时，交通流可以从上游连接转移到下游连接。当上游连接过度饱和时，转移率等于饱和率，当两个相邻连接之间没有通道时，转移率被认为为 0。因此，当上游过度饱和时，通过相应通道转移的飞机数量是绿灯时间与饱和流率的乘积 (考虑了飞行间隔)。对于接合点 j_i 的飞行过程集合 FD_i ，存在 $fd_i^{ab} \in FD_i$ ，其中 fd_i^{ab} 是从输入连接 l_i^a 到输出连接 $l_i^b, l_i^a \in L_{in}(j_i), l_i^b \in L_{out}(j_i)$ 的交通流。每个接合点都有多种交通流转移过程 $L_{in}(j_i) \times L_{out}(j_i)$ ，这些过程由不同的相位控制以供使用。p_i^k 表示过渡接合点的第 k 个相位，j_i, P_i 是接合点 j_i 的所有相位的集合。

$$FD_i = L_{\text{in}}(j_i) \times L_{\text{out}}(j_i) = \left\{fd_i^{ab}\right\} \tag{3}$$

$$P_i = \left\{p_i^1, \cdots, p_i^k, \cdots p_i^K\right\} \tag{4}$$

2.2. Cyclic phase backpressure control traffic signal control at junctions

2.2. 周期相位背压控制交通信号控制法在交叉口的运用

To realize the adaptive control at junctions of MVS-TA, this paper describes the queuing process of junctions based on the dynamic queuing model, and calculates the allowable pass time for each phase by using the Cycle Phase Backpressure (CPB) policy adapted to the flight operation.

为了实现 MVS-TA 交叉口的自适应控制，本文基于动态排队模型描述了交叉口的排队过程，并使用适应于飞行操作的周期相位背压 (CPB) 策略计算了每个相位的允许通过时间。

In the control model, the time parameters are modeled as discrete, i.e., based on a slotted time model. $tp = 1, 2, \cdots$ represents the number of the period about to be initiated. Assuming that the cycle length of each transit junction is TP , each link has only one flight path. Control decisions in CPB policy are made at the beginning of each time cycle (so it is a fixed cycle policy which is similar to the policy in (Le et al., 2015)). At the beginning of each control cycle, the ground navigation device can update the data in the next cycle, including the queue data and the green time assigned to each phase p_i^k . Compared with ground traffic, due to the need to control the interval of flights passing through intersections, the buffer time of traffic lights is not set, that is, the total period length is equal to the effective period length.

在控制模型中，时间参数被建模为离散的，即基于分时时间模型。$tp = 1, 2, \cdots$ 表示即将启动的周期数。假设每个过渡接点的周期长度为 TP ，每个链接只有一个飞行路径。在 CPB 策略中，控制决策在每个时间周期的开始时进行 (因此它是一个固定周期策略，类似于 (Le et al., 2015) 中的策略)。在每个控制周期的开始，地面导航设备可以更新下一个周期中的数据，包括队列数据和分配给每个相位的绿灯时间 p_i^k 。与地面交通相比，由于需要控制飞机通过交叉点的间隔，交通灯的缓冲时间没有设置，即总周期长度等于有效周期长度。

2.2.1. Queue dynamics model

2.2.1. 队列动力学模型

References to relevant literature (Hao, 2019; Le et al., 2015; Ma et al., 2020), this section provides a quantitative description of the dynamic queuing model on the air route. For junction j_i , at the beginning of the tp window, the number of aircraft queuing on link l_i^a and entering link l_i^b is $Q_{ab}(tp)$, and the total number of aircraft queued on link l_i^a is $Q_a(tp)$, which means:

参考相关文献 (Hao, 2019; Le et al., 2015; Ma et al., 2020)，本节提供了对航空路由上动态队列模型的定量描述。对于接点 j_i ，在 tp 窗口开始时，链接 l_i^a 上排队和进入链接 l_i^b 的飞机数量为 $Q_{ab}(tp)$ ，链接 l_i^a 上排队的飞机总数为 $Q_a(tp)$ ，这意味着:

$$Q_a(tp) = \sum_{l_i^b \in L_{out}(j_i)} Q_{ab}(tp) \tag{5}$$

At the beginning of the $tp+1$ window, the number of aircraft queued on link l_i^a and entered link l_i^b, $Q_{ab}(tp+1)$, can be expressed as:

在 $tp+1$ 窗口开始时，链接 l_i^a 上排队的飞机数量和进入 link l_i^b, $Q_{ab}(tp+1)$ 的数量可以表示为:

$$Q_{ab}(tp+1) = Q_{ab}(tp) - \{\text{ The number of flights flying from } l_i^a \text{ to } l_i^b \text{ during } tp \text{ period. }\}$$

$+\{$ The ratio of the flight flying from l_i^a to $l_i^b \cdot\} * \{$ During tp period, the upstream links increase the number of flights on $l_i^a\}$

$+\{$ The ratio of the flight flying from l_i^a to $l_i^b \cdot\} * \{$ During tp 周期，上游链接增加了 $l_i^a\}$ 上的航班数量。

$\varphi_{p_i^k}(\mathfrak{p})$ is the proportion of green light time of the phase p_i^k controlling traffic fd_i^{ab} , and this value calculation will be detailed in section 2.2.2. If link l_l^a is saturated during tpperiod, the number of aircraft from l_l^a to l_l^b is the product of the rate $SR_{ab}(tp)$ and the corresponding phase time allowed, otherwise the value is $Q_{ab}(tp)$. Therefore, $Q_{ab}(tp+1)$ can be quantified as:

$\varphi_{p_i^k}(\mathfrak{p})$ 是相位 p_i^k 控制交通 fd_i^{ab} 的绿灯时间比例，这个值的计算将在第 2.2.2 节中详细说明。如果在 tpperiod 期间，链接 l_l^a 达到饱和，那么从 l_l^a 到 l_l^b 的飞机数量是速率 $SR_{ab}(tp)$ 与相应相位允许时间的乘积，否则该值为 $Q_{ab}(tp)$ 。因此，$Q_{ab}(tp+1)$ 可以量化为:

$$Q_{ab}(tp+1) = Q_{ab}(tp) - \left\{\left[SR_{ab}(tp) \cdot \varphi_{\mathrm{p}_i^*}(\mathrm{tp}) \cdot \mathrm{TP}\right] \wedge \mathrm{Q_{ab}}(\mathrm{tp})\right\} + \mathrm{R_{ab}}(\mathrm{tp}) \sum_{\mathrm{c} \in \Gamma_{\mathrm{a}}^+} \left\{\left[\mathrm{SR_{ca}}(\mathrm{tp}) \cdot \varphi_{\mathrm{p}_i^*}(\mathrm{tp}) \cdot \mathrm{TP}\right] \wedge \mathrm{Q_{ca}}(\mathrm{tp})\right\} \tag{6}$$

Where, define $\mathrm{x} \wedge \mathrm{y} = \min(\mathrm{x}, \mathrm{y})$. For $fd_i^{ab} \in FD_i, R_{ab}(tp)$ is the turning rate, i.e. the ratio of the number of vehicles entering l_i^b from l_i^a luring cycle tp to the total number of vehicles on l_i^a , which satisfies $\sum_{l_i^b \in L_{out}(j_i)} R_{ab}(tp) = 1$.

其中，定义 $\mathrm{x} \wedge \mathrm{y} = \min(\mathrm{x}, \mathrm{y})$ 。对于 $fd_i^{ab} \in FD_i, R_{ab}(tp)$ 是转向率，即从 l_i^a 进入 l_i^b 的车辆数与 l_i^a 上总车辆数的比率，这满足 $\sum_{l_i^b \in L_{out}(j_i)} R_{ab}(tp) = 1$ 。

The turning ratio for vehicles entering link l_i^a within cycle tp cannot be calculated at the beginning of the cycle (Ma et al.,2020). Assuming that the upstream link of the intersection is equally likely to enter each downstream link, the initial value of this parameter is estimated. Based on the homogeneity of aircraft (Le et al.,2015), the value of $R_{ab}(\mathfrak{p})$ is updated in the process of simulation. The homogeneity of aircraft means each car at the junction has the same likelihood of joining each subsequent junction. When the system collects a large amount of flight operation data in practice, it is available to determine the stable value of $R_{ab}(tp)$ at different times of the day.

在周期 tp 开始时，无法计算进入链接 l_i^a 的车辆的转向比率 (Ma et al.,2020)。假设交叉口的上游链接有相等的概率进入每个下游链接，估计该参数的初始值。基于飞机的同质性 (Le et al.,2015)，在模拟过程中更新 $R_{ab}(\mathfrak{p})$ 的值。飞机的同质性意味着在每个交叉口的每辆车加入下一个交叉口的概率相同。当系统在实际情况中收集了大量飞行操作数据时，可以确定一天中不同时间的 $R_{ab}(tp)$ 的稳定值。

$$R_{ab}(tp) = \frac{1}{N} \sum_{tp=1}^{tp} \frac{QL_{ab}(tp)}{QL_a(tp)} \tag{7}$$

tp is the current cycle number. $QL_{ab}(tp)$ and $QL_a(tp)$ are the number of flights in the tp period that are sent by link l_i^a to the link l_i^b and the total number of flights on the l_i^a link, respectively. N is the number of periods used to calculate the probability of turning.

tp 是当前周期数。$QL_{ab}(tp)$ 和 $QL_a(tp)$ 分别是 tp 期间由链接 l_i^a 发送到链接 l_i^b 的飞机数量和 l_i^a 链接上的总飞机数量。N 是用于计算转向概率的周期数。

2.2.2. Cyclic phase backpressure control policy-traffic control rules at junctions

2.2.2. 循环相位背压控制策略-交叉口的交通控制规则

Backpressure control policies were originally developed by (Tassiulas and Ephremides, 1992) for routing and scheduling of packet

背压控制策略最初由 (Tassiulas 和 Ephremides，1992) 为无线网络中的数据包路由和调度而开发。

transmission in a wireless network. Later, backpressure strategies were used to control traffic signals for urban ground traffic(Varaiya, 2013a, 2013b; Wongpiromsarn et al., 2012). This section uses the backpressure policy with fixed cycle time and cyclic phases to control the traffic flow at the intersection, which is an improved control method of the original strategy. The main advantage of the CPB control policy is: 1) Unlike centralized optimization structures with high traffic and computation, this strategy is a distributed optimization control method that requires traffic flow control based on information about the appropriate control points and adjacent links. 2) This strategy can obtain traffic network feedback in real-time and dynamically adjust the signal control scheme at the beginning of each cycle to optimize intersection throughput (Le et al., 2015).

后来，背压策略被用于控制城市地面交通的信号灯 (Varaiya，2013a，2013b；Wongpiromsarn 等，2012)。本节使用具有固定周期时间和循环相位的背压策略来控制交叉口的交通流，这是对原始策略的改进控制方法。CPB 控制策略的主要优点是:1) 与具有高交通和计算量的集中优化结构不同，这种策略是一种分布式优化控制方法，需要基于关于适当控制点和相邻链路的信息进行交通流控制。2) 这种策略可以实时获取交通网络反馈，并在每个周期开始时动态调整信号控制方案，以优化交叉口的吞吐量 (Le 等，2015)。

Similar to ground transportation, a signal control that manages traffic flow in different directions is defined as a phase. The system control is based on the communication navigation monitoring network. The total time required to complete a set of signal indications in each traffic flow direction is called the cycle length of the intersection. The transit junction is an important node to control the traffic flow and reduce the collision risk from the mechanism. According to the traffic volume of different phases, CPB strategy can allocate more allowed passing time for the phases with large traffic flow in each period, and realize the maximum throughput and stable control of the traffic network.

与地面交通类似，管理不同方向交通流的信号控制被定义为一个相位。系统控制基于通信导航监测网络。完成每个交通流方向的信号指示所需的总时间称为交叉口的周期长度。交通枢纽是控制交通流和降低碰撞风险的重要节点。根据不同相位的交通量，CPB 策略可以为每个时段交通流量大的相位分配更多的允许通行时间，实现交通网络的最大吞吐量和稳定控制。

Because the CNS network can monitor the number of aircraft queuing at each intersection in real-time, the CPB policy controls traffic based on the queue length. For the same intersection, the larger the backpressure weight of the phase, the longer the passing time assigned. According to the queue length, turn probability and saturation flow rate, the backpressure weight and the proportion of green time of the next period are calculated at the beginning of each cycle.

由于 CNS 网络能够实时监控每个交叉口中排队的飞机数量，CPB 策略基于队列长度控制交通。对于同一交叉口，相位的反向压力权重越大，分配的通过时间越长。根据队列长度、转向概率和饱和流量，在每个周期开始时计算下一时期的反向压力权重和绿灯时间的比例。

The calculation process of CPB policy is as follows:

CPB 策略的计算过程如下:

During the tp period, the pressure weight generated by traffic flow fd_i^{ab} is the queue length $Q_{ab}\left(tp\right)$ at l_i^a minus the average queue length at the output link l_i^b , which can be expressed as

在 tp 期间，由交通流 fd_i^{ab} 产生的压力权重是 l_i^a 的队列长度 $Q_{ab}\left(tp\right)$ 减去输出 link l_i^b 的平均队列长度，可以表示为

$$\text{pressure}_{ab}\left(tp\right) = Q_{ab}\left(tp\right) - \sum_{c \in out_b} R_{ab}\left(tp\right) \cdot \mathrm{Q_{bc}}\left(\mathrm{tp}\right) \tag{8}$$

During the tp period, the pressure weight of p_i^k (the kth phase of the transit junction j_i) is accumulated by the pressure weight of traffic flows controlled by that phase (Eq. (9)).

在 tp 期间，p_i^k (交通枢纽 j_i 的第 k 个相位) 的压力权重是由该相位控制的交通流的压力权重累积而成 (公式 (9))。

$$W_{p_i^k}\left(tp\right) = \sum_{fd_i^{ab} \in p_i^k} \text{pressure}_{ab}\left(tp\right) \cdot \mathrm{SR_{ab}}\left(\mathrm{tp}\right) \tag{9}$$

According to the backpressure weight of each phase at the beginning of the current period of the intersection, the division ratio of the green time of each phase can be calculated. The proportion of green light time of each phase p_i^k can be expressed as Eq. (10).

根据当前周期开始时交叉口每个相位的反向压力权重，可以计算每个相位的绿灯时间分配比例。每个相位的绿灯时间比例 p_i^k 可以表示为公式 (10)。

$$\varphi_{p_i^k}\left(tp\right) = \frac{\exp\left[\eta \bullet W_{p_i^k}\left(tp\right)\right]}{\sum\limits_{p_i^* \in P_i} \exp\left[\eta \bullet W_{p_i^*}\left(tp\right)\right]} \tag{10}$$

Each weight value can be positive or negative, and the green light time ratio is always positive. You can adjust η by adjusting the parameters and parameters. The green light time ratio for each phase of junction j_i is satisfied Eq. (11).

每个权重值可以是正的或负的，而绿灯时间比例总是正的。可以通过调整参数和参数来调整 η。交叉口每个相位的绿灯时间比例满足公式 (11)。

$$\sum_{p_i^k \in P_i} \varphi_{p_i^k}(tp) = 1 \tag{11}$$

Assuming that the aircraft on each link comes from its upstream link, the remaining capacity of link l_l^a at the beginning of the period $tp+1$ is directly related to the flight flow of the upstream link $f_a^{in}(tp)$ and the downstream link $f_a^{out}(tp)$ in tp period, where $f_a^{in}(tp)$ and $f_a^{\text{out}}(tp)$ are calculated similarly to Eq. (6).

假设每条链路上的飞机来自其上游链路，周期开始时链路 l_l^a 的剩余容量直接与上游链路 $f_a^{in}(tp)$ 在 tp 期间的飞行流量和下游链路 $f_a^{out}(tp)$ 相关，其中 $f_a^{in}(tp)$ 和 $f_a^{\text{out}}(tp)$ 的计算类似于公式 (6)。

$$QL_a(tp+1) = \min\left\{QL_a(tp) + f_a^{in}(tp) - f_a^{out}(tp), C_a^{\max}\right\} \tag{12}$$

$$C_a^{\text{rem}}(tp+1) = C_a^{\max} - QL_a(tp+1)$$

$$f_a^{in}(tp) = \sum_{c \in \Gamma_a^+} \{[SR_{ca}(tp) \cdot GT_{ac}(tp)] \wedge [QL_c(tp) \cdot R_{ca}(tp)]\} \tag{13}$$

$$GT_{ac}(tp) = \varphi_{p_i^k}(tp) \cdot TP, fd_i^{ac} \in p_i^k$$

$$f_a^{\text{out}}(tp) = \sum_{b \in \Gamma_a^-} \{[SR_{ab}(tp) \bullet \text{GT}_{\text{ab}}(\text{tp})] \wedge [\text{QL}_{\text{a}}(\text{tp}) * \text{R}_{\text{ab}}(\text{tp})]\} \tag{14}$$

Where $C_a^{\max}$ represents the maximum capacity (capacity threshold) of the link, C_a^{rem} (tp) represents the remaining capacity of link l_i^a at the beginning of cycle tp.Γ_a^+ and Γ_a^- represent the upstream-link collection of link l_i^a and the downstream-link collection of link l_i^a , respectively. $QL_a(tp)$ is the total traffic of segment l_i^a of the tp period. Flights from l_i^a to l_i^b are controlled by the appropriate phase at the intersection. $GT_{ab}(tp)$ represents the allowed pass time (green light time) for that phase during the tp period.

其中 $C_a^{\max}$ 表示链路的最大容量 (容量阈值)，C_a^{rem} (tp) 表示在周期 tp.Γ_a^+ 开始时链路 l_i^a 的剩余容量，Γ_a^- 分别代表链路 l_i^a 的上游链路集合和下游链路集合，$QL_a(tp)$ 是 tp 时期段 l_i^a 的总流量。从 l_i^a 到 l_i^b 的航班由交叉口的适当相位控制。$GT_{ab}(tp)$ 表示在该相位期间允许的通行时间 (绿灯时间)。

It is important to note that the usual fixed phase sequence control method has a minimum green light pass time limit for each phase,

需要注意的是，通常的固定相位序列控制方法为每个相位设定了最少的绿灯通行时间限制，

i.e. the phase where the link is about to overflow (the backpressure weight is very small) is also assigned a minimum green time (Ma et al., 2020), which is not allowed in the safety-demanding terminal area scheduling. Because the location of the aircraft and the load of each link can be monitored with the CNS network, the remaining capacity of the air traffic link can be quantified more accurately. This paper takes into account the capacity limitations of each link: 1) the minimum green light pass time is not considered in the allocation of green time for each phase; 2)The number of flights passing through each phase should be satisfied Eq. 15, and overloaded flights need to wait at intersections or choose other routes. The junctions shall control that the load of each link is less than its maximum capacity $(QL_a(tp) \le C_a^{\max})$, and the load of the corresponding ring layer is also less than its capacity threshold.

即即将溢出的链路所在的相位 (背压权重非常小) 也被分配了最少的绿灯时间 (Ma et al., 2020)，这在安全要求高的终端区调度中是不允许的。因为飞机的位置和每个链路的负载可以通过 CNS 网络进行监控，所以可以更准确地量化空中交通链路的剩余容量。本文考虑了每个链路的容量限制:1) 在为每个相位分配绿灯时间时，不考虑最少的绿灯通行时间；2) 每个相位通过的航班数量应满足等式 15，并且超载航班需要在交叉口等待或选择其他路线。交叉口应控制每个链路的负载小于其最大容量 $(QL_a(tp) \le C_a^{\max})$ ，并且相应环层的负载也小于其容量阈值。

$$\sum_{fd_i^{ab} \in p_i^k} QG_{ab}(tp) \le C_b^{\max} - QL_b(tp) \tag{15}$$

Where $QG_{ab}(tp)$ is the number of flights allowed through the phase p_i^k in tp cycle.

其中 $QG_{ab}(tp)$ 是在 tp 周期内允许通过相位 p_i^k 的航班数量。

3.The integrated adaptive scheduling model for approach-departure flights

3. 进近-起飞航班的集成自适应调度模型

3.1. Problem description

3.1. 问题描述

The integrated adaptive scheduling model to solve the problem is: Based on the operating characteristics of eVTOL and the designed operating environment, how to schedule and optimize the operation of flights in the terminal area to minimize the cost of flight delay.

集成的自适应调度模型用于解决问题如下: 基于 eVTOL 的运行特性及设计的运行环境，如何调度和优化终端区域内的航班运行，以最小化航班延误成本。

In this section, the adaptive control model of MVS-TA is proposed, including two sub-models, which are the shortest path planning model based on the dynamic traffic network and the distributed sequencing at junctions. Given the destination vertiport and the boundary point from the terminal area, each aircraft can dynamically adjust the flight path and pass through the intersections in sequence and at intervals. It is worth noting that the traditional flight scheduling method is usually to sort and optimize all flights throughout the optimization period, and the calculation pressure is relatively large in the case of large flight volume. The adaptive control model in this article is calculated for queued flights at each intersection. The implementation of distributed optimization can greatly reduce the control pressure of the central controller.

在本节中，提出了 MVS-TA 的自适应控制模型，包括两个子模型，分别是基于动态交通网络的 shortest path 规划模型和交叉口的分布式排序。给定目的地的垂起机场和终端区域的边界点，每架飞机可以动态调整飞行路径并依次通过交叉口并保持间隔。需要注意的是，传统的航班调度方法通常是在整个优化期间对所有航班进行排序和优化，当航班量大时计算压力相对较大。本文中的自适应控制模型是对每个交叉口排队航班进行计算。分布式优化的实施可以大大减轻中央控制器的控制压力。

The model built in this article is based on the following premises:

本文构建的模型基于以下前提:

(1) In this paper, it is considered that flight collisions can be avoided, and safety can be ensured through safe separation and intersection rules, as well as the CNS network. The risk assessment of the terminal area is not within the scope of this paper.

(1) 本文认为可以通过安全间隔和交叉口规则以及 CNS 网络来避免飞行冲突并确保安全。终端区域的风险评估不在本文讨论范围内。

(2) The model constructed is aimed at flight scheduling in the MVS-TA, without considering the number of vertipads in the ver-tiport. Under the premise of not considering the scheduling between vertipads, the model can also be applied to the terminal-area scheduling of a single vertiport with multiple vertipads.

(2) 构建的模型针对的是 MVS-TA 中的航班调度，未考虑垂起机场中的垂起垫数量。在不考虑垂起垫之间调度的前提下，模型也可应用于单个垂起机场内多个垂起垫的终端区域调度。

(3) The terminal area scheduling structure of this paper is set to medium flight density, and the capacity limit of Holding Stack is not considered.

(3) 本文设置的终端区域调度结构为中等航班密度，未考虑等待栈的容量限制。

Based on the traffic network structure and control rules of the transit junction of the MVS-TA, combined with the operating characteristics of eVTOL, this section constructs the integrated adaptive scheduling model as follows:

基于 MVS-TA 的过渡交叉口交通网络结构和控制规则，结合 eVTOL 的运行特性，本节构建了以下综合自适应调度模型:

3.2.The shortest path planning model based on the dynamic traffic network

3.2. 基于动态交通网络的 shortest 路径规划模型

eVTOL as a vehicle and mobile load carrier, its travel distribution and route selection will affect the operation efficiency of the terminal area route, while the remaining electricity, range, etc. will affect the safety level of the system. On the other hand, the topology and control rules of the traffic network in the terminal area will affect the path planning of eVTOL from the ground base station. Therefore, ”eVTOL state- path planning - control rules ” are related and affected by each other. Based on MVS-TA structure and intersection control rules, this section puts

forward the update mechanism of dynamic traffic network, depicts the effect of terminal segment traffic on eVTOL running time, and constructs the shortest route planning model based on dynamic traffic network.

eVTOL 作为一种车辆和移动载具，其旅行分布和路线选择将影响终端区域路线的运行效率，而剩余电量、航程等将影响系统的安全水平。另一方面，终端区域交通网络的拓扑结构和控制规则将影响 eVTOL 从地面基站的路径规划。因此，”eVTOL 状态 - 路径规划 - 控制规则” 是相互关联并相互影响的。基于 MVS-TA 结构和交叉口控制规则，本节提出了动态交通网络的更新机制，描述了终端段交通对 eVTOL 运行时间的影响，并构建了基于动态交通网络的 shortest 路径规划模型。

3.2.1. Dynamic traffic network modeling

3.2.1. 动态交通网络建模

(1) Route impedance model

(1) 路径阻抗模型

First, the road resistance function is constructed to describe the cost of the flight during the approach and departure. Based on the commonality of air traffic and ground traffic, as well as the correlation between traffic flow speed-flow-density, the basic relationship between traffic flow and travel time can be obtained. (Hao, 2017; Sun, 2020; Wang et al., 2006; Xu et al., 2015):

首先，构建道路阻抗函数来描述飞行过程中的接近和离开成本。基于空中交通和地面交通的共性，以及交通流速度-流量-密度之间的相关性，可以得到交通流与旅行时间的基本关系。(Hao, 2017; Sun, 2020; Wang et al., 2006; Xu et al., 2015):

$$t = t_0 \left(\frac{2}{1 + \sqrt{1 - \frac{q}{C}}} \right) \tag{16}$$

Traffic flow represents the number of traffic entities passing through a segment or section during a period, the value of which is constantly changing with time and space, and the traffic flow at a certain time is not of sufficient practical significance. This paper selects the traffic network real-time update mechanism with tp as the update cycle(Cui,2013), so the average $\overline{QL_a}$ and saturation $S_a\left(tp\right)$ (Eq. (17)) are calculated by the flow of the adjacent period of l_l^a . The road resistance of segment l_l^a updated in the cycle tp can be further available (Eq. (18)).

交通流量表示在一段时间内通过某一区段或路段的交通实体数量，其值随时间和空间不断变化，某一特定时间的交通流量并不具有足够的实际意义。本文选择以 tp 作为更新周期 (Cui,2013) 的交通网络实时更新机制，因此平均 $\overline{QL_a}$ 和饱和度 $S_a\left(tp\right)$ (公式 (17)) 是通过 l_l^a 相邻周期的流量来计算的。在周期 tp 中更新的路段 l_l^a 的道路阻力可以进一步得到 (公式 (18))。

$$S_a\left(tp\right) = \frac{\overline{QL_a}}{C_a^{\max}} = \frac{\left[QL_a\left(tp\right) + QL_a\left(tp+1\right)\right]}{C_a^{\max} \cdot 2}, \left(tp-1\right)TP \le st_j^f \le tp \cdot \mathrm{TP} \tag{17}$$

$$W_{ij}\left(tp\right) = t_0 \left(\frac{2}{1 - \sqrt{1 - S_a\left(tp\right)}} \right) \tag{18}$$

$S_a\left(\mathrm{tp}\right)$ indicates the saturation of segment l_i^a in the period to which time st_j^f belongs, which is the ratio of the average traffic volume to the capacity of the corresponding route, and $S_a\left(tp\right) \le 1$. s t_j^f indicates the time at which the aircraft f reaches the transit junction j_i . If condition $\left(tp-1\right)TP \le st_j^f \le tp \cdot \mathrm{TP}$ is met, st_j^f belongs to the tp cycle.

$S_a\left(\mathrm{tp}\right)$ 表示属于时间 st_j^f 的周期内路段 l_i^a 的饱和度，即相应路线的平均交通量与路线容量之比，以及 $S_a\left(tp\right) \le 1$ 。s t_j^f 表示飞机 f 到达中转接点 j_i 的时间。如果满足条件 $\left(tp-1\right)TP \le st_j^f \le tp \cdot \mathrm{TP}$ ，则 st_j^f 属于 tp 周期。

(2) The traffic network topology of MVS-TA

(2) MVS-TA 的交通网络拓扑结构

Taking the road resistance as the weight, the route network of MVS-TA is constructed by a topological relationship, with nodes (such as v_k, v_q) representing intersections and arcs representing the connections of each road.

以道路阻力作为权重，通过拓扑关系构建 MVS-TA 的路由网络，其中节点 (例如 v_k, v_q) 表示交叉口，弧表示每条道路的连接。

The route network is defined as $\mathbf{G}^T = (\mathbf{V}, \mathbf{E}, \mathbf{A}, \mathbf{C})$, where **V** is the set of nodes, **A** is the road weight set, **C** is the capacity of the road, **E** is the collection of all the curved segments, that is, the collection of all segments in the terminal area.

路由网络定义为 $\mathbf{G}^T = (\mathbf{V}, \mathbf{E}, \mathbf{A}, \mathbf{C})$ ，其中 **V** 是节点集合，**A** 是道路权重集合，**C** 是道路容量，**E** 是所有曲线段的集合，即终端区域中所有路段的集合。

$$a_{kq} = \begin{cases} w_{kq}(tp), v_{kq} \in E, \text{ the resistance of } v_{kq} \\ 0, v_k = v_q \\ \infty, v_{kq} \notin E \text{ or Reach the threshold of } v_{kq} \end{cases} \tag{19}$$

$\mathbf{A} = (a_{kq})_{K \times K}$ describes the road lengths, the connections of the nodes, the one-way or two-way access, and the road resistance characteristics. The segment of the terminal area in this paper is one-way access. Its element value $\mathbf{w}_{kq}(tp)$ is updated with the number of flights on the corresponding road. Adjacent matrix A can be generally expressed as Eq. (20) (Luo et al.,2016).

" $\mathbf{A} = (a_{kq})_{K \times K}$ 描述了道路长度、节点的连接、单向或双向通行以及道路阻力特性。本文中终端区域的路段为单向通行。其元素值 $\mathbf{w}_{kq}(tp)$ 随着对应道路上航班数量的更新而更新。邻接矩阵 A 通常可以表示为公式 (20) (Luo et al.,2016) 的形式。"

$$\mathbf{A} = \begin{bmatrix} 0 & w_{12}(tp) & w_{13}(tp) & \cdots & w_{1K}(tp) \\ w_{21}(tp) & 0 & w_{23}(tp) & \cdots & w_{2K}(tp) \\ w_{31}(tp) & w_{32}(tp) & 0 & \cdots & w_{3K}(tp) \\ \vdots & \vdots & \vdots & \ddots & \vdots \\ w_{K1}(tp) & w_{K2}(tp) & w_{K3}(tp) & \cdots & 0 \end{bmatrix} \tag{20}$$

Therefore, $\mathbf{G}^T$ can be expressed as Eq. (21).

" 因此，$\mathbf{G}^T$ 可以表示为公式 (21)。"

$$\begin{cases} \mathbf{G}^T = (\mathbf{V}, \mathbf{E}, \mathbf{A}, \mathbf{C}) \\ \mathbf{V} = \{v_k \mid k = 1, 2, \cdots, K\} \\ \mathbf{E} = \{v_{kq} \mid v_k \in \mathbf{V}, v_q \in \mathbf{V}, k \neq q\} \\ \mathbf{A} = \left\{ w_{kq}(tp) \mid v_{kq} \in \mathbf{E}, (tp-1)\,TP \leq st_j^f \leq tp \cdot TP \right\} \\ \mathbf{C} = \{G_\alpha^{max} \mid a \in L\} \end{cases} \tag{21}$$

3.2.2.The shortest path planning model

"##### 3.2.2. 最短路径规划模型"

Based on the section 3.2.1, the road resistance of each section varies dynamically with the change of saturation, which can realize the real-time update of the traffic network. When the aircraft reaches each transit junction, the system plans and guides its path from the current position $L_s(f)$ to the destination $L_d(f)$. The time at which the aircraft reaches its current position is st_f^f . The time for the aircraft to arrive at the destination $t_d(f)$ is the accumulation of the road resistance of the actual driving path $R_p(f)$:

" 基于 3.2.1 节，每个路段的道路阻力随着饱和度的变化而动态变化，从而实现交通网络的实时更新。当飞机到达每个中转节点时，系统会从当前位置 $L_s(f)$ 规划并引导飞机至目的地的路径 $L_d(f)$ 。飞机到达当前位置的时间是 st_f^f 。飞机到达目的地的时间 $t_d(f)$ 是实际行驶路径上道路阻力的累积 $R_p(f)$ 。"

$$t_d(f) = st_j^f + \sum_{v_{ij} \in R_p(f)} (v_{kq} \cdot \mathrm{w_{kq}(tp)}) \tag{22}$$

$$v_{kq} = \begin{cases} 1, v_{kq} \in R_p(f) \\ 0, v_{kq} \notin R_p(f) \end{cases} \tag{23}$$

Table 1

" 表 1"

three-dimensional priority of flights.

" 航班的立体优先级。"

	State of Charge R = 1		State of Charge R = 2		State of Charge R = 3	
	Approach O = 1	Departure O = 2	Approach O = 1	Departure O = 2	Approach O = 1	Departure O = 2
mission characteristics V = 1	1	2	4	8	10	18
mission characteristics V = 2	3	6	9	16	19	31

	电量状态 R = 1		电量状态 R = 2		电量状态 R = 3	
	方法 O = 1	出发 O = 2	方法 O = 1	出发 O = 2	方法 O = 1	出发 O = 2
任务特性 V = 1	1	2	4	8	10	18
任务特性 V = 2	3	6	9	16	19	31

In the current route network state, seek the shortest time path planning for each flight from the current point to its destination to determine the next node and the next route to be flying, which can be expressed as Eq. (24).

" 在当前路由网络状态下，为每架航班寻求从当前位置到目的地的最短时间路径规划，以确定下一个节点和下一条飞行路径，可以表示为公式 (24)。"

$$\min W_f = \min t_d(f) = \min\left(st_j^f + \sum_{v_{kq}\in R_p(f)} (v_{kq}\cdot \mathrm{w_{kq}(tp)})\right) \tag{24}$$

3.3. Distributed scheduling model for flights at junctions

"### 3.3. 交叉点处航班的分布式调度模型"

3.3.1. Objective function

"#### 3.3.1. 目标函数"

The position adjustment involved in the sorting work will bring some control load and risk to the aircraft, so the aircraft sorting work is completed within the waiting time of the intersection. Transit junction is the key node in the flight path, not only to update the shortest-time path according to traffic network obstruction, but also to sort the queue for flights according to the importance. Considering the safety, the goal of the model proposed in this paper is to minimize the total comprehensive running time through each transit intersection under the constraints of the safe interval, take-off and landing interval, and battery charge state.

在排序工作中涉及的位置调整会给飞机带来一定的控制负荷和风险，因此飞机的排序工作需要在交叉点的等待时间内完成。过渡节点是飞行路径中的关键节点，不仅要根据交通网络阻塞更新最短时间路径，还要根据航班的重要性对航班队列进行排序。考虑到安全性，本文提出的模型目标是，在安全间隔、起飞和降落间隔以及电池充电状态的约束下，通过每个过渡交叉点的总综合运行时间最小化。

The number of flights waiting to pass through junction j is n_F^j . Flight f arrives at the terminal area at ETA_f and is allowed to pass junction j at et_f^j . The combined operating time of each flight at each junction can be expressed as Eq. (25).

等待通过交叉点 j 的航班数量为 n_F^j 。航班 f 在 ETA_f 到达终端区域，并允许在 et_f^j 通过交叉点 j 。每个航班在每个交叉点的综合运行时间可以表示为公式 (25)。

$$\mathrm{Delay}_f^j = \mathrm{Imp}_f\left(st_f^j\right)\cdot\left|\mathrm{et_f^j} - \mathrm{ETA_f}\right|, \mathrm{f} = 1,2,\cdots,\mathrm{n_F^j}; \forall \mathrm{j}\in \mathrm{J} \tag{25}$$

$$\mathrm{Im}\, p_f(t) = \left\lceil M/\mathrm{prior}_f(t)\right\rceil \tag{26}$$

$Imp_f(t)$ is the important factor of flight f at the moment t , which is related to the flight's approach-departure attribute, mission characteristics and the State Of Charge (SOC), and is reflected by the priority $\mathrm{prior}_f(t)$ of the flight. M is the largest number in the priority table (Table 1). In this section, the time parameter t is measured as a moment node in the timeline (intervals of 1 s), t ∈ T .

$Imp_f(t)$ 是航班 f 在时刻 t 的重要因素，它与航班的起降属性、任务特性以及充电状态 (SOC) 有关，并通过航班的优先级 $\mathrm{prior}_f(t)$ 反映出来。M 是优先级表 (表 1) 中的最大数值。在本节中，时间参数 t 被测量为时间线上的一个时刻节点 (1 s 的间隔)，t ∈ T 。

The optimization goal of sequencing is to minimize the combined running time of queued flights at the junction:

航班排序的优化目标是最小化在交叉点排队航班的总运行时间。

$$\min\sum_{f=1}^{n_F^j}\mathrm{Delay}_f^j = \min\sum_{f=1}^{n_F^j}\mathrm{Imp}_f\left(st_f^j\right)\bullet\left|\mathrm{et_f^j} - \mathrm{ETA_f}\right|, \mathrm{f} = 1,2,\cdots,\mathrm{n_F^j}, \forall \mathrm{j}\in \mathrm{J} \tag{27}$$

3.3.2. Constraints

3.3.2. 约束条件

Since the green pass time for each phase, i.e., the pass window, is limited, the ordering of the current phase can end when the optimized departure time et_f^j of the last flight in the sorted flight exceeds the pass window boundary of the next signal cycle. The remaining unsorted flights need to wait for the next cycle red light and sort.

由于每个阶段的绿灯通行时间，即通行窗口，是有限的，当前阶段的排序可以在优化后的最后一个排序航班的起飞时间 et_f^j 超过下一个信号周期的通行窗口边界时结束。剩余的未排序航班需要等待下一个周期的红灯并排序。

Assuming that eVTOL flight power consumption increases linearly over travel time, ground base stations can obtain the SOC of aircraft f in real time. The aircraft's SOC is $SOC_f\left(st_f^j\right)$ when arriving at junction j . This parameter tracks the status of the vehicle's power from full $(1.0, 100\%)$ to empty(0.0), which can be expressed as Eq. (28).

假设 eVTOL 飞行功率消耗随飞行时间线性增加，地面基站可以实时获取飞机的 SOC f 。飞机到达交点 j 时的 SOC 为 $SOC_f\left(st_f^j\right)$ 。这个参数跟踪了车辆从满电 $(1.0, 100\%)$ 到耗尽 (0.0) 的电力状态，可以用公式 (28) 表示。

$$SOC_f\left(st_f^j\right)=\gamma\left(SOC_f^0-E_c\cdot\left(\mathrm{ETA_f}-\mathrm{st_f^j}\right)\right) \tag{28}$$

γ is the energy consumption factor, the value range is $[0.9, 1]$ .SOC_f^0 is the SOC of flight f when entering the terminal area. E_c is the power consumption per unit time (s) of the aircraft.

γ 是能量消耗系数，其取值范围是 $[0.9, 1]$ .SOC_f^0 是飞机进入终端区域时的 SOC f 。E_c 是飞机每单位时间 (秒) 的功耗。

$$ES_f\left(st_f^j\right)+EP_{fj}-1\leq EQ_{fj} \tag{29a}$$

$$\left[ES_f\left(st_f^j\right)+EP_{fj}\right]/2\geq EQ_{fj} \tag{29b}$$

$$et_{f'}^j+\delta_{ff'}-M'\left(1-w_{f,f'}\rho_{f,f'}\right)\leq et_f^j,\forall f,f'\in \mathrm{F};\forall \mathrm{j}\in \mathrm{J} \tag{29c}$$

$$ST_{u,f'}+\sigma_{ff'}-M'\left(1-\lambda_{f,f'}\rho_{f,f'}\right)\leq ST_{u,f},\forall f,f'\in \mathrm{F};\forall \mathrm{u}\in \mathrm{U} \tag{29d}$$

$$et_f^j-GS_{p_j^k}(f)\geq M'\left(\text{ ord }-1\right),\forall f\in \mathrm{F};\forall \mathrm{j}\in \mathrm{J} \tag{29e}$$

$$P_{ef}^j-P_{sf}^j\leq P^R,\forall f\in F;\forall j\in \mathrm{J} \tag{29f}$$

$$P_{sf}^j-P_{ef}^j\leq P^R,\forall f\in F;\forall j\in \mathrm{J} \tag{29g}$$

$$\begin{cases}\text{ if } EQ_{fj}=0, et_f^j=st_f^j\\ \text{ if } EQ_{fj}=1, P_{sf}^j\geq 1, P_{ef}^j\geq 1\end{cases} \tag{29h}$$

The constraints on the scheduling model of queued flights at each intersection are as follows:

每个交叉点排队航班调度模型的约束条件如下:

Assuming that flight f reaches the intersection j during the tp period, and the direction of the next route is controlled by phase $p_j^k, GS_{p_j^*}(f,tp)$ is the green

假设航班 f 在 tp 期间到达交点 j ，并且下一条路线的方向由相位 $p_j^k, GS_{p_j^*}(f,tp)$ 控制，此时为绿灯。

$$EP_{fj}=\begin{cases}1, \text{ if } st_f^j<GS_{p_j^k}(f,tp) \text{ or } st_f^j\geq G_{p_j^k}(f,tp)+GS_{p_j^k}(f,tp), \text{ or } Q_{ab}\left(st_f^j\right)\neq 0\\ 0, \text{ otherwise}\end{cases}$$

$$\forall j\in \mathrm{J}, (tp-1)\,TP\leq st_j^f\leq tp\cdot \mathrm{TP}$$

$$\rho_{f,f} = \begin{cases} 1, & \text{if flight } f' \text{ is in the adjacent previous position of flight } f \\ 0, & \text{otherwise} \end{cases}$$

$$w_{f,f} = \begin{cases} 1, \text{ if flight } f \text{ and } f \text{ are at the same intersection} \\ 0, \text{ otherwise} \end{cases}$$

$$\lambda_{f,f} = \begin{cases} 1, \text{ if flight } f \text{ shares the same vertiport with } f' \\ 0, \text{ otherwise} \end{cases}$$

$$EQ_{fj} = \begin{cases} 1, \text{ if flight } f \text{ is required to queue at intersection } j \\ 0, \text{ otherwise} \end{cases}$$

$$\text{ord } = \begin{cases} 1, \text{ Flight } f \text{ is the first in the queue } \left(P_{sf}^{j} = 1\right) \\ 0, \text{ otherwise} \end{cases}$$

Decision variables
决策变量
Constraints
约束条件

Eq. (29a) - (29b) determines whether flight f is queued according to the SOC and the arrival time at the junction, which are constraints related to the queue status of intersection j . If the SOC of flight f is less than 16% , or the flight has other unexpected conditions, ES_f is 0 . The flight is dispatched to the emergency ring floor and can be reached directly to the planned airport without having to wait in line. For flights with SOC greater than 10% , if the phase at the junction is green and there are no queued flights at st_f^1 , $EP_{fj} = 0$, it can pass at the specified interval. Otherwise, the flight will need to be suspended waiting in line and the service system will sort the waiting list. When $ES_f\left(st_f^j\right) = 1$ and $EP_{fj} = 1$, flight f waits at junction j (Eq.29a).

公式 (29a)-(29b) 根据飞机的 SOC 和在交叉点的到达时间确定航班 f 是否排队，这些是与交叉点队列状态相关的约束。如果航班 f 的 SOC 小于 16%，或者飞机有其他意外情况，ES_f 为 0。该航班将被调度到紧急环层，可以直接到达预定机场而无需排队等待。对于 SOC 大于 10% 的航班，如果交叉点的相位为绿灯且 st_f^1 没有排队的航班，$EP_{fj} = 0$，则可以在指定间隔通过。否则，航班将需要暂停等待排队，服务系统将对等待列表进行排序。当 $ES_f\left(st_f^j\right) = 1$ 且 $EP_{fj} = 1$ 时，航班 f 在交叉点 j 等待 (公式 29a)。

Eq. (29c) ensure that the adjacent waiting flight f and f at junction j meet the separation requirements (Separation Norms). Eq. (29d) is the interval constraint of vertiport $u.M$ is an infinite positive number. Eq. (29e) ensures that the first flight in the order leaves the intersection at the time after the green light $GS_{p_j^k}(f)$ of the next period in the corresponding phase p_j^k . Considering the safety and ensuring that flights are not delayed too long due to sequencing, the queuing position adjustment constraint of flight f at junction j is described by Eq. (29f) and Eq. (29g). Eq. (29h) describes the relationship between EQ_{fj}, et_f^j and P_{sf}^j

式 (29c) 确保在连接点 f 相邻的等待航班 f 满足间隔要求 (间隔规范)。式 (29d) 是机场 $u.M$ 的时间间隔约束，是一个无限正数。式 (29e) 确保顺序中的第一个航班在相应相位 p_j^k 的下一个周期的绿灯 $GS_{p_j^k}(f)$ 之后离开交叉点。考虑到安全并确保航班由于排序而不会延误过长，航班 f 在连接点 j 的排队位置调整约束由式 (29f) 和式 (29g) 描述。式 (29h) 描述了 EQ_{fj}, et_f^j 与 P_{sf}^j 之间的关系。

When optimizing flight order at intersections, the differences in priority levels due to the flight's specific attributes must be considered. This paper calculates the main factors of priority from the SOC, mission characteristics and the mode of operation (takeoff/landing). Considering the characteristics of the dynamic change of the SOC over time parameters, this paper creatively transforms the relatively static priority factor (Wen and Huo, 2020; Zhang and Yang, 2018) into a comprehensive dynamic priority factor for flights. Flights with smaller priority factors have a higher priority in queuing optimization.

在优化交叉点的航班顺序时，必须考虑由于航班特定属性导致的优先级差异。本文从 SOC、任务特性以及操作模式 (起飞/着陆) 计算了优先级的主要因素。考虑到 SOC 随时间参数的动态变化特性，本文创造性地将相对静态的优先级因素 (Wen 和 Huo，2020；Zhang 和 Yang，2018) 转化为航班的综合动态优先级因素。优先级因素较小的航班在排队优化中具有更高的优先级。

Specifically, the characteristic parameters of flight f have a direct impact on its priority. The state of charge, mission characteristics, the operation mode is represented as R_f, V_f, O_f , respectively. The priority of flight f at time t is $\text{prior}_f(t)$. According to the importance of the three characteristic parameters (SOC $>$ mission characteristics $>$ operation mode), the priority is calculated by using Eq. (34) (Wang et al., 2004).

具体来说, 航班 f 的特征参数直接影响其优先级。电荷状态、任务特性、操作模式分别表示为 R_f, V_f, O_f 。航班 f 在时间 t 的优先级为 $\text{prior}_f(t)$ 。根据三个特征参数 (SOC > 任务特性 > 操作模式) 的重要性，使用式 (34)(Wang 等，2004) 计算优先级。

Waiting for the aircraft in the queue at the junction to sort at a certain tailing interval, to ensure the fairness of flight priority calculation, the location node of the first aircraft as a reference to correct the power load status SOC_f^* (Eq. (30)). To prevent excessive discharge of the battery, 10% is considered a battery protection threshold (Kleinbekman et al.,2020). The power consumed by the path from the nearest and farthest boundary points to the vertiports is used as the level 1 priority boundary (Eq. (31)).

在交叉点处的队列中等待飞机按照一定的尾流间隔进行排序，以确保航班优先级计算的公平性，以第一架飞机的位置节点作为参考来校正功率负载状态 SOC_f^* (式 (30))。为了防止电池过度放电，10% 被视为电池保护阈值 (Kleinbekman et al., 2020)。从最近和最远的边界点到垂直起降场的路径消耗的功率被用作一级优先级边界 (式 (31))。

$$SOC_{fj}^* = \text{SOC}\left(st_f^j\right) - P_{sf}^j - 1\delta_{ff}, E_c \tag{30}$$

$$R_f(t) = \begin{cases} 1, 16\% \le \text{SOC}_{fj}^* < 32\% \\ 2, 32\% \le \text{SOC}_{fj}^* < 66\% \\ 3, 66\% \le \text{SOC}_{fj}^* < 100\% \end{cases} \tag{31}$$

$$V_f = \begin{cases} 1, & \text{Urgent tasks} \\ 2, & \text{Otherwise} \end{cases} \tag{32}$$

$$O_f = \begin{cases} 1, \text{ approach} \\ 2, \text{ departure} \end{cases} \tag{33}$$

$$\text{prior}_f(t) = \text{PRIOR}\left(R_f(t), V_f, O_f\right) = \frac{\left(\text{pri}_f(t)-1\right)\left(\text{pri}_f(t)-2\right)\left(\text{pri}_f(t)-3\right)}{6} + \frac{\left(2\text{pri}_f(t) - R_f(t) - 2\right)\left(R_f(t)-1\right)}{2} + V_f \tag{34}$$

And
并且

$$\text{pri}_f(t) = R_f(t) + V_f + O_f$$

For example, if flight 1 is an approaching flight on an emergency mission and SOC_1^* is 25% , i.e. $R_1 = 1, V_1 = 1, O_f = 1$, then flight 1 has priority $\text{prior}_1 = \text{PRIOR}(R_1, V_1, O_1) = 1$. Similarly, a three-dimensional priority table for flights can be derived (Table1).

例如，如果航班 1 是一次执行紧急任务的进近航班且 SOC_1^* 是 25% , 即 $R_1 = 1, V_1 = 1, O_f = 1$, 那么航班 1 具有优先权先于 $_1 = \text{PRIOR}(R_1, V_1, O_1) = 1$ 。类似地，可以为航班制定一个三维优先级表 (表 1)。

4. Description of the algorithmic process

4. 算法过程描述

The adaptive control strategy for the scheduling of approach-departure flights in MVS-TA includes two parts: the construction of the operating environment and operating rules, and the integrated adaptive scheduling model (Fig. 5). The specific process of the adaptive scheduling optimization part is as follows (Fig. 6):

在 MVS-TA 中进离场航班调度自适应控制策略包括两部分: 构建运行环境和运行规则，以及综合自适应调度模型 (图 5)。自适应调度优化部分的具体过程如下 (图 6):

(1) Initialization of information parameters: topology of the traffic network in the terminal area, allowed pass time (green time) for each phase of the first cycle, road traffic, road impedance, and basic information about the flight (including initial point, destination, initial power, mission characteristics., mode of operation, etc.).

(1) 信息参数初始化: 终端区域交通网络的拓扑结构，第一个周期内每个阶段的允许通行时间 (绿灯时间)，道路交通，道路阻抗，以及航班的基本信息 (包括起始点、目的地、初始功率、任务特性、运行模式等)。

(2) Data update of the operating environment: At the beginning of the tp cycle, update the segment traffic $QL_a(tp+1)$, junction green light ratio $\varphi_{p_t^k}(tp+1)$ of tp , as well as the segment impedance $w_{ij}(tp)$. At the end of the tp cycle, record the queue length $Q_a(tp)$ and segment traffic $QL_a(tp)$ of tp , and update the turn probability $R_{ab}(tp)$ according to the queuing data.

(2) 操作环境数据更新: 在 tp 周期开始时，更新路段流量 $QL_a\,(tp+1)$ 、路口绿灯比例 $\varphi_{p_t^k}\,(tp+1)$ 以及路段阻抗 $w_{ij}\,(tp)$ 。在 tp 周期结束时，记录路口的队列长度 $Q_a\,(tp)$ 和路段流量 $QL_a\,(tp)$ ，并根据排队数据更新转向概率 $R_{ab}\,(tp)$ 。

(3) Minimum time path planning:When a flight reaches each transit junction, with minimal impedance W_f as the optimization target, the Dijkstra algorithm is used to calculate the shortest-time path and determine the next junction and segment.

(3) 最短时间路径规划: 当航班到达每个中转路口时，以最小阻抗 W_f 为优化目标，使用迪杰斯特拉算法计算最短时间路径并确定下一个路口和路段。

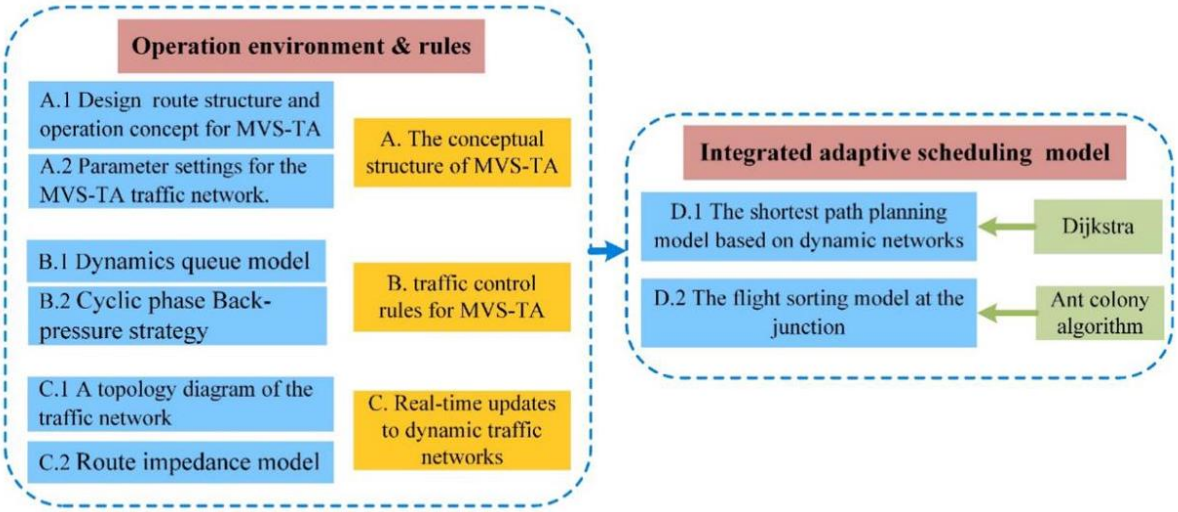

Fig. 5. The overall framework of the adaptive control strategy in MVS-TA.
图 5. MVS-TA 中自适应控制策略的总体框架。

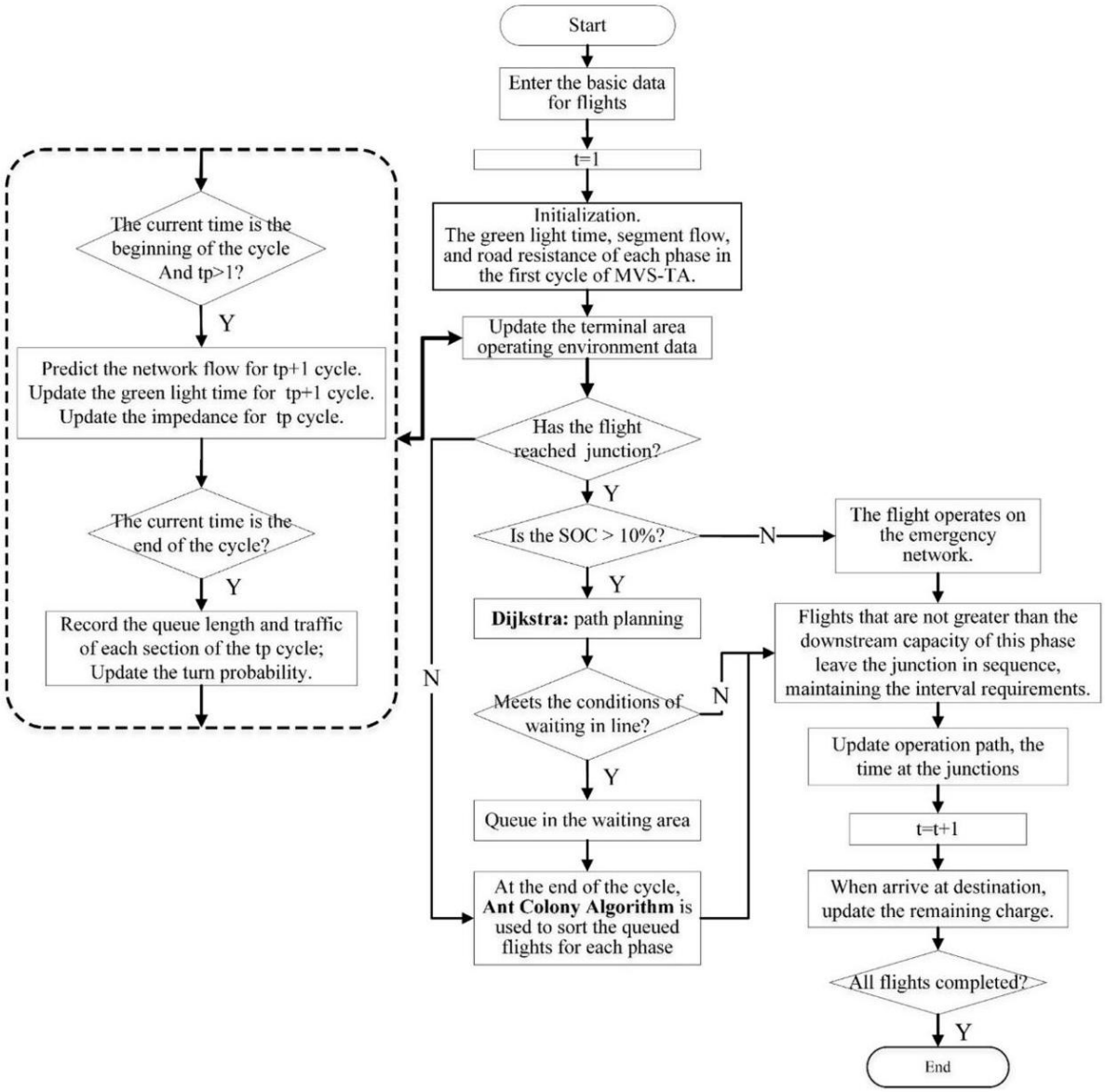

Fig. 6. The process of adaptive control strategy algorithm.

图 6. 自适应控制策略算法的过程。

(4) Waiting and sequencing at the junction: Determine the phase that controls the passage of a flight based on the next running section updated. Flights with less than 10% of the remaining power are operating on the emergency ring. Flights that meet (29a) (29b) will need to be suspended waiting in line until the phase is allowed to pass. At the end of each cycle, to minimize the weighted time $\text{Delay}_f^i\left(st_f^i\right)$ through the junction, the Ant Colony Algorithm (ACO) is used to sort the queued flights so that the more important flights can pass through the junction first. The flight will continue to wait until the next cycle if the following occurs: 1) the optimized passage time of the flight exceeds the green pass time range of the phase. 2) The capacity of the next route to be remitted has reached the upper limit.

(4) 路口等待与排序: 根据更新的下一个运行路段确定控制航班通行的相位。剩余电量少于 10% 的航班在紧急环道上运行。满足 (29a) (29b) 条件的航班需要暂停排队等待，直到允许通行。在每个周期结束时，为了最小化通过路口的加权时间 $\text{Delay}_f^i\left(st_f^i\right)$，使用蚁群算法 (ACO) 对排队航班进行排序，使得重要航班能够优先通过路口。如果出现以下情况，航班将继续等待直到下一个周期:1) 航班的优化通行时间超过了相位的绿灯通行时间范围。2) 下一跳要发送的路线容量已达到上限。

(5) System scheduling judgment: scheduling all flights introduced by the system. Exit scheduling when all flights have completed route planning and end the operation in the terminal area (approach flights arrive at the vertiports, departure flights leave the outer ring layer).

(5) 系统调度判断: 调度系统引入的所有航班。当所有航班完成航线规划并结束终端区操作 (进近航班到达垂起机场，出发航班离开外环层) 时退出调度。

5. Numerical examples and result analysis

5. 数值示例与结果分析

5.1. Experiment scenario settings

5.1. 实验场景设置

(1) Aircraft-related parameter settings (see Table 2): Take the Ehang 216, an aircraft with 16 propellers that can carry two people for experimental simulation, the cruise speed is 130 km/h (about 36.1 m/s). In this paper, the cruising speed is set at 36 m/s , the horizontal speed $v_x = 8$ m/s at altitude drop (Stages (2)-(3) and (5)-(6) in Fig. 9), the vertical speed is variable. The speed of the vertical take-off and landing phase (stage (9)in Fig. 9) is 3 m/s , and assume that eVTOL can operate continuously for 1 hour (EHANG216, n.d.; Kleinbekman et al., 2018). (Cotton, 2019) studied the design separation values between multiple types of aircraft (manned/unmanned eVTOL, VFR/IFR/AFR, etc.) and concluded that the longitudinal interval between unmanned eVTOLs with passengers could be as low as 300ft. (Bosson and Lauderdale, 2018) use the spatial separation criteria of 0.3 nmi and 100ft as simulation scenarios. Based on the above research, this paper sets the distance interval of 0.3 nmi (about 555.6 m , interval of about 15 s) when the aircraft cruises, and calculates the maximum capacity of the route. Taking into account the FAA's interval requirements for F-class aircraft (less than 15,400 lb) (Bosson and Lauderdale, 2018; Federal Aviation Administration, 2016), this paper sets the time interval between the aircraft's sequencing at the junction and vertiport to 60 s, taking into account the complex operating scenarios of the junction.

(1) 飞机相关参数设置 (见表 2): 以 Ehang 216 为例，这是一种带有 16 个螺旋桨的飞机，能够搭载两人进行实验模拟，巡航速度为 130 km/h (大约 36.1 m/s)。在本文中，将巡航速度设置为 36 m/s ，在高度下降阶段 (图 9 中的阶段 (2)-(3) 和 (5)-(6))，水平速度 $v_x = 8$ m/s 是变化的。垂直起降阶段 (图 9 中的阶段 (9)) 的速度为 3 m/s ，并假设 eVTOL 能够连续运行 1 小时 (EHANG216，n.d.；Kleinbekman 等人，2018 年)。(Cotton，2019) 研究了多种类型飞机 (有人/无人 eVTOL，VFR/IFR/AFR 等) 之间的设计间隔值，并得出结论，载客无人 eVTOL 之间的纵向间隔可以低至 300 英尺。(Bosson 和 Lauderdale，2018) 使用 0.3 nmi 和 100 英尺的空间间隔标准作为模拟场景。基于以上研究，本文在飞机巡航时设置 0.3 nmi (大约 555.6 m ，间隔大约 15 s) 的距离间隔，并计算航线的最大容量。考虑到美国联邦航空局 (FAA) 对 F 类飞机 (小于 15,400 磅) 的间隔要求 (Bosson 和 Lauderdale，2018；联邦航空局，2016 年)，本文将飞机在交接点和垂起机场的排序时间间隔设置为 60 秒，考虑到交接点的复杂运行场景。

By adjusting the proportion of the cruise stage (flying at cruising speed) during the down/climbing phase, the energy consumption of the eVTOL can be optimized and is conducive to the avoidance of high-rise buildings (Kleinbekman et al., 2018). In the experimental scenario settings, the proportion of the horizontal running phase of the flight at cruising speed is 60% of the drop/climb phase (for example, stage (2) in Fig. 9 accounts for 60% of the drop stage (2)-(3)).

通过在下降/爬升阶段调整巡航阶段 (以巡航速度飞行) 的比例，可以优化 eVTOL 的能耗，并有利于避开高层建筑 (Kleinbekman et al., 2018)。在实验场景设置中，飞行在巡航速度下的水平滑跑阶段的比例是下降/爬升阶段 60% (例如，图 9 中的阶段 (2) 占下降阶段 (2)-(3) 的 60%)。

(2) The parameter settings for the operational environment (see Table 3 and 4): The operating environment includes the setting of terminal area structure and control rules. An application structure of the conceptual structure of MVS-TA proposed in this paper can be constructed as shown in Fig. 7. According to (Bertram and Wei, 2020; Kleinbekman et al., 2018), setting the radius of Ring_A, Ring_B , and Ring_C to 3500 m, 2000 m , and 600 m , respectively. The emergency ring layer has a radius of 1000 m , the same horizontal plane as Ring_C , and the vertical distance between the plane and the landing site is 200 m . The terminal area concept is converted into a traffic topology map for simulation, where the traffic path topology on the approach side is shown in Fig. 8. In practice, the parameters in the MVS-TA conceptual structure and control rules need to be adjusted according to the actual operating conditions.

(2) 操作环境的参数设置 (见表 3 和 4): 操作环境包括终端区域结构和控制规则的设置。本文提出的 MVS-TA 概念结构的应用结构可以构建如图 7 所示。根据 (Bertram 和 Wei, 2020; Kleinbekman et al., 2018)，设置 Ring_A, Ring_B 的半径为 Ring_C ，3500 m, 2000 m 分别为 600 m 和 1000 m 。紧急环层的半径为 200 m ，与 Ring_C 处于同一水平面，平面与着陆点之间的垂直距离为 [latex6] 。终端区域概念被转换成用于模拟的交通拓扑图，其中接近侧的交通路径拓扑如图 8 所示。在实际中，根据实际运行条件，需要调整 MVS-TA 概念结构和控制规则中的参数。

Compared with the adaptive terminal area system, it is the traditional terminal area airspace structure applied to civil aviation (Fig. 10). To ensure the validity of the comparison results, the ring layer parameters and the position of the points of the traditional airspace structure are basically the same as between the adaptive terminal area structure, but there is no emergency ring layer. There are no points controlled by the signal light in the airspace structure. The approach- departure fixes are only distributed in the outermost ring layer.

与自适应终端区域系统相比，它是应用于民航的传统终端区域空域结构 (见图 10)。为确保比较结果的有效性，传统空域结构的环层参数和点的位置与自适应终端区域结构基本相同，但不存在应急环层。在空域结构中，没有由信号灯控制的点。进近-起飞定位点仅分布在最外环层。

(3) The adaptive control system (ACS) and the traditional control system (TCS): The implementation of ACS relies on the signal control based on the backpressure strategy and integrated adaptive model. The advantage is that the adaptive control and distributed control of the busy systems can be realized, the flight path and sequence can be optimized, and the flight with high importance can end the terminal area operation stage first.

(3) 自适应控制系统 (ACS) 与传统控制系统 (TCS):ACS 的实施依赖于基于背压策略的信号控制和集成的自适应模型。其优点在于可以实现繁忙系统的自适应控制和分布式控制，优化飞行路径和序列，使重要航班能够首先结束终端区域操作阶段。

Since civil airliners cannot hover during the voyage, if the terminal area is saturated, traditional air traffic management usually adopts the strategy of air and ground waiting to dispatch flights. Under the constraints of separation, sector capacity, runway usage separation, airport service capability, etc., the approach-departure flights are scheduled and sorted. The flights that are not authorized to enter (or leave) the terminal area are subject to waiting at the holding pattern (or airport). The characteristics of the traditional airspace structure and control strategy are that 1) there is a fixed route between the approach-departure fixes and the vertiport, and 2) the flight cannot change the route determined during the flight. Referring to the flight optimization study of civil aviation's regional multi-airport system (Shao et al., 2020; Zhang et al., 2017), the baseline model can be represented as Eq. (35)-Eq. 36.

由于民用客机在航行中无法悬停，如果终端区域饱和，传统空中交通管理通常采用空中和地面等待策略来调度航班。在分离、扇区容量、跑道使用分离、机场服务能力等约束下，对进近-起飞航班进行计划安排和排序。未经授权进入 (或离开) 终端区域的航班需在等待航线 (或机场) 等待。传统空域结构和控制策略的特点是:1) 进近-起飞定位点与直升机场之间有固定航线；2) 飞行中不能改变确定的航线。参照民用航空区域多机场系统的飞行优化研究 (Shao 等人，2020；Zhang 等人，2017)，基线模型可以表示为公式 (35)-公式 36。

$$\min\left(\sum_{f\in F}\left(ET_f - ST_f\right)\right)$$

$$\text{s.t. } \left(FA_u\left(t\right), FD_u\left(t\right)\right) \in CR_u\left(t\right), \forall u \in U, \forall t \in T \tag{36a}$$

$$FS_s\left(t\right) \le CS_s\left(t\right), \forall s \in S, \forall t \in T \tag{36b}$$

$$w_{ff'}\rho_{ff'}\left(LPT_{f'} + \delta_{ff'}\right) \le LPT_f, \forall f, f' \in F \tag{36c}$$

$$\lambda_{ff}\cdot\rho_{ff}\left(ET_f + \sigma_{ff}\right) \le ET_f, \forall f, f' \in F \tag{36d}$$

$$ETA_f \le ET_f, \forall f \in F \tag{36e}$$

Table 2
表 2
eVTOL operating parameters and separation settings.
eVTOL 运行参数和分离设置。

Operation parameters				Cruising separation	Junction separation	Take-off and landing separation
Cruising speed	The speed at height drops	Vertical speed	Endurable time			
36 m/s	$v_x = 8$ m/s, v_y variable	3 m/s	1 h	15 s	60 s	60 s

操作参数				巡航间隔	连接处间隔	起飞与降落间隔
巡航速度	高度下降速度	垂直速度	耐久时间			
36 m/s	$v_x = 8$ m/s, v_y 变量	3 m/s	1 h	15 s	60 s	60 s

Table 3
表 3
Parameter Settings of adaptive control system.
自适应控制系统的参数设置。

Relevant parameters of transit junction		Vertiport capacity		
Time periodTP	Backpressure parameter η	Vertiport 1	Vertiport 2	Vertiport 3
120 s	40	20	20	20

过渡连接处的相关参数		垂直机场容量		
时间周期 TP	反压参数 η	垂直起降场 1	垂直起降场 2	垂直起降场 3
120 s	40	20	20	20

Table 4
表 4
Parameter setting of traditional control system.
传统控制系统的参数设置。

Sector capacity				Vertiport capacity			The separation at the junctions	Take-off and landing separation
Sector1	Sector2	Sector3	Sector4	Vertiport1	Vertiport2	Vertiport3		
30	25	25	25	20	20	20	60 s	60 s

扇区容量				垂直起降场容量			在交汇处的分离	起飞与着陆的分离
扇区 1	扇区 2	Sector3	Sector4	垂直机场 1	垂直机场 2	垂直机场 3		
30	25	25	25	20	20	20	60 s	60 s

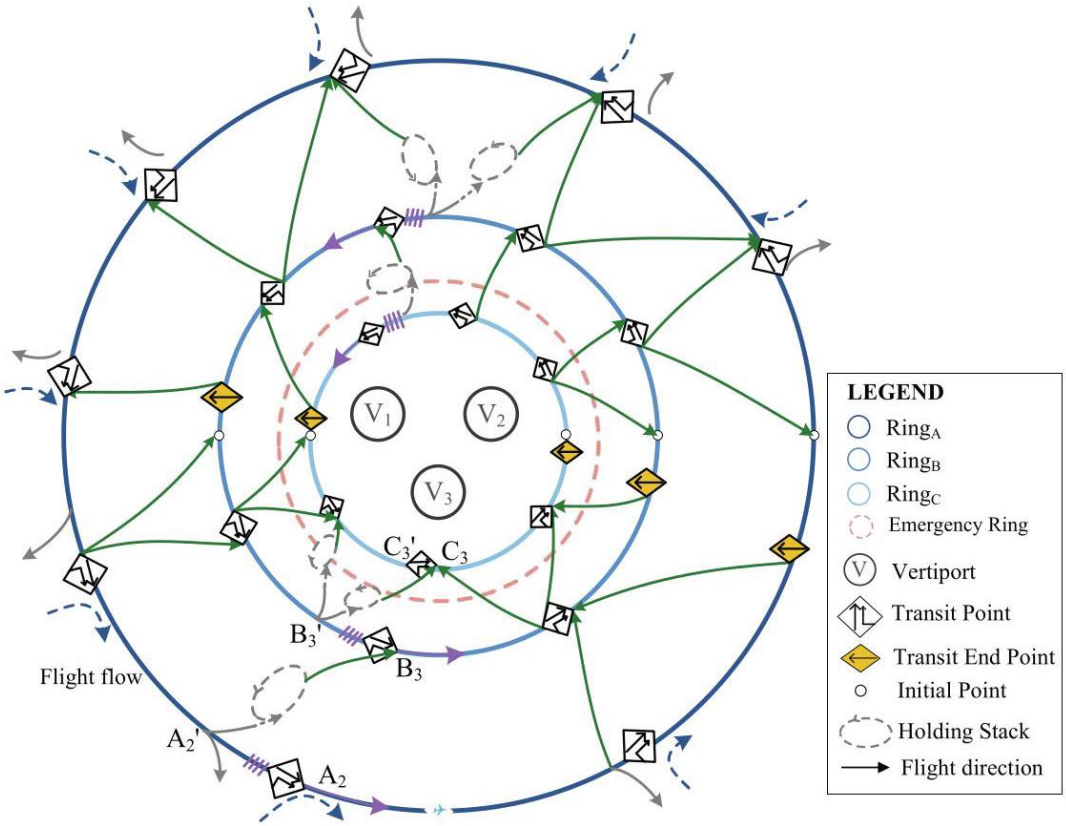

Fig. 7. Terminal area structure diagram of MVS.
图 7. MVS 终端区域结构图。

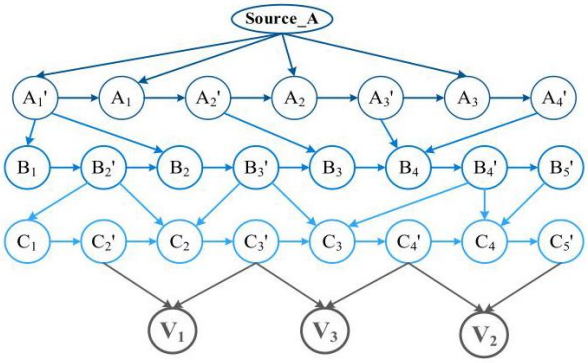

Fig. 8. The topology of the approach side traffic network.
图 8. 接近侧交通网络的拓扑结构。

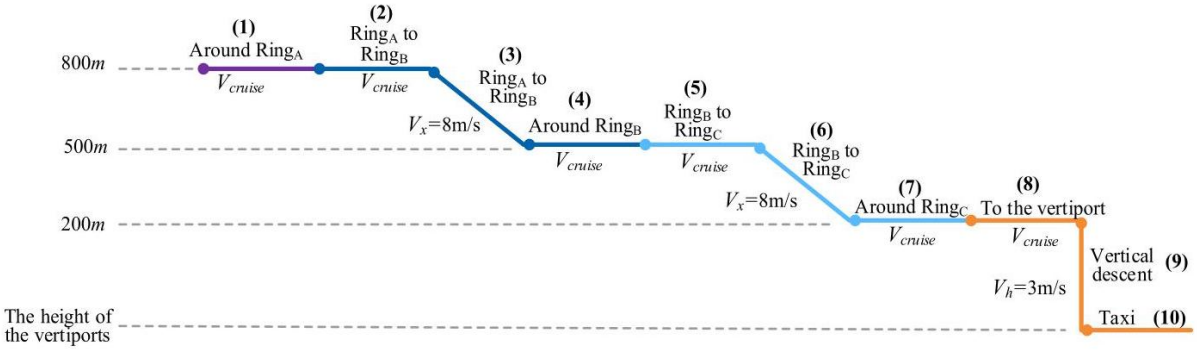

Fig. 9. Sectional view of the flight approach process.
图 9. 飞行进近过程的剖面图。

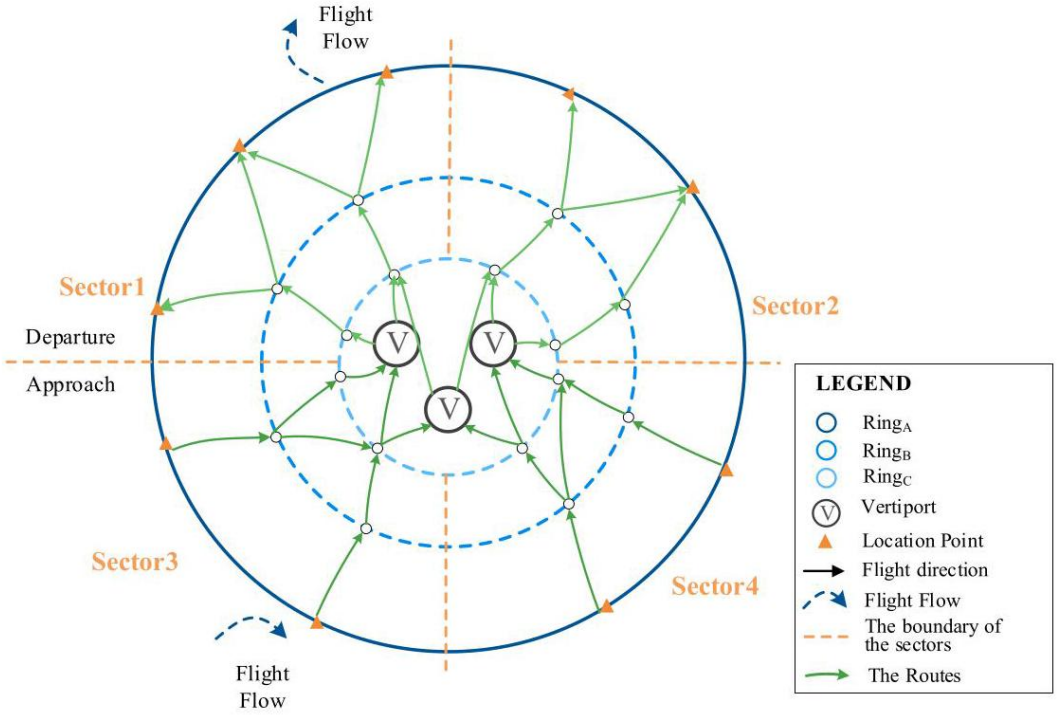

Fig. 10. Airspace structure of the traditional terminal area.

图 10. 传统终端区的空域结构。
Table 5
表 5。
Parameter settings in ACO.
ACO 中的参数设置。

Parameter	α	β	ρ	Q	Number of iterations
Value-ACS	1	5	0.3	100	300
Value-TCS	1	5	0.1	300	2500

参数	α	β	ρ	Q	迭代次数
价值-ACS	1	5	0.3	100	300
价值-TCS	1	5	0.1	300	2500

The optimization is to minimize the sum of all flight delays. ET_f and ST_f are the target runway time and estimated runway time of the flight f , respectively. Eq. (36a) are the vertiport capacity constraints, which mean that arrival flow $FA_u(t)$ and departure flow $FD_u(t)$ at the vertiport u during period t should meet the capacity constraint $CR_u(t)$. Eq. (36b) are the sector capacity constraints, which require that arrival-departure flights of the sector s during the period $t(FS_s(t))$ must satisfied the capacity $CS_s(t)$. Eq. (36c) ensure that the separation of the adjacent flight f and f' , where $\delta_{ff'}$ represents the minimum safety separation. If flight f' is in the adjacent previous position of flight f, ρ_{ff} is valued at 1, otherwise 0 . If flight f and its previous flight f are through the same location, w_{ff} value is 1, otherwise 0 . Similarly, the Eq.(36d) is the separation constraint at vertiport u , where σ_{ff} represents the minimum safety separation and ET_f is the landing/take-off time of flight f . If flight f shares the same vertiport with f , λ_{ff} is valued at 1, otherwise it is 0 . Eq. (36e) are time window constraints, which mean that the target runway time (ET_f) is greater than the minimum boundary (time to reach the system) ETA_f .

优化是为了最小化所有航班延误的总和。ET_f 和 ST_f 分别是目标跑道时间和预计跑道时间 f 。式 (36a) 是直升机场容量约束，意味着在时间段 t 内，直升机场 u 的到达流量 $FA_u(t)$ 和出发流量 $FD_u(t)$ 应满足容量约束 $CR_u(t)$ 。式 (36b) 是扇区容量约束，要求在时间段 $t(FS_s(t))$ 内，扇区 s 的到达-出发航班必须满足容量 $CS_s(t)$ 。式 (36c) 确保相邻航班 f 和 f' 之间的间隔，其中 $\delta_{ff'}$ 表示最小安全间隔。如果航班 f' 位于航班 f, ρ_{ff} 的相邻前位置，则取值为 1，否则为 0。如果航班 f 和其前一个航班 f 通过相同位置，则 w_{ff} 的值为 1，否则为 0。同样，式 (36d) 是直升机场 u 的间隔约束，其中 σ_{ff} 表示最小安全间隔，ET_f 是航班 f 的着陆/起飞时间。如果航班 f 与 f 共享同一直升机场，则 λ_{ff} 的值为 1，否则为 0。式 (36e) 是时间窗口约束，意味着目标跑道时间 (ET_f) 大于最小边界 (到达系统的时间) ETA_f 。

(4) Parameter setting of ACO: In this paper, the ACO is used to solve two problems, one is the optimization of queued flights at the intersection of ACS, and the other is the sorting of flights under TCS, that is, the baseline problem. Based on the general ACO, the algorithm used in this paper gives priority to low-power flights in each iteration and retains the optimal solution to the next iteration. According to (Duan, 2005), the best experience of parameter settings in the Ant-Cycle model of ACO is as follows: $0 \leq \alpha \leq 5; 0 \leq \beta \leq 5; 0.1 \leq \rho \leq 0.99; 10 \leq \mathrm{Q} \leq 10000$.

(4) ACO 参数设置: 本文使用 ACO 解决两个问题，一个是 ACS 交叉口的排队航班优化问题，另一个是 TCS 下的航班排序问题，即基线问题。基于通用 ACO 算法，本文使用的算法在每次迭代中优先考虑低能耗航班，并将最优解保留到下一次迭代。根据 (Duan, 2005) 的研究经验，ACO 的 Ant-Cycle 模型的最佳参数设置如下: $0 \leq \alpha \leq 5; 0 \leq \beta \leq 5; 0.1 \leq \rho \leq 0.99; 10 \leq \mathrm{Q} \leq 10000$ 。

The parameter of ACO in this paper are set according to the experience of research (Duan, 2005) (Wu et al., 2016), see Table 5.

本文中的 ACO 参数设置是根据 (Duan, 2005) (Wu et al., 2016) 的研究经验进行的，见表 5。

5.2. Results analysis

5.2. 结果分析

To validate the performance of the proposed MVS-TA structure and scheduling strategy, a computational study based on a variety of scenarios was carried out and the results are presented in this section. In section 5.2.1, the performance of ACS and TCS is compared. In section 5.2.2, the effect of the characteristics of flight entry into the terminal area on ACS operating performance is explored. Section 5.2.3 further analyzes the performance of ACS in random arrival scenarios. Given the actual application scenario, approach flights are about 1.5 times the number of departure flights, and the demand of the three vertiports is relatively evenly distributed.

为了验证所提出的多垂直起降场 (MVS-TA) 结构和调度策略的性能，本文进行了基于多种场景的计算研究，并在本节中呈现结果。在 5.2.1 节中，比较了 ACS 和 TCS 的性能。在 5.2.2 节中，探讨了航班进入终端区域的特点对 ACS 运行性能的影响。5.2.3 节进一步分析了随机到达场景下 ACS 的性能。考虑到实际应用场景，进近航班大约是起飞航班数量的 1.5 倍，且三个垂直起降场的需求相对均匀分布。

It should be noted that: 1) The time that eVTOL enter the terminal area (ETA) refers to the arrival of the approach-flight to the outer ring boundary or departure flight ready to take off. 2) The end of the terminal area operation phase refers to the arrival of approaching flights to the vertiport or departure flights leaving the outer ring layer of the terminal are. 3) The flight entry interval reflects the density of the flight to be sorted.

应该注意的是:1) eVTOL 进入终端区域的时间 (ETA) 指的是进近航班到达外环边界或起飞航班准备起飞的时间。2) 终端区域操作阶段结束指的是进近航班到达垂直机场或起飞航班离开终端区域的外环层。3) 航班进入间隔反映了待排序航班的密度。

5.2.1. Performance of ACS and TCS for multi-vertiport

5.2.1. 多垂直机场的 ACS 和 TCS 性能

To compare the performance of the two systems with different terminal area structures and control strategies, this paper sets up an instance scenario with the flight volume to be sorted as $10/20/\ldots/100$, and assumes that ETA intervals are subject to the Poisson distribution of $\lambda = 60$. The initial power of approaching flights is normally distributed with an average of 35% and a standard deviation of 5%, while the initial power of departure flights is normally distributed with an average of 92% and a standard deviation of 2.5%. The calculation of ACS and TCS is based on the algorithm framework (Fig. 6) and ACO, respectively. Fig. 11 shows the average flight time of TCS in scenarios where the number of flights is 20 and 40, with a maximum difference of 14.82% and 28.70%, respectively. Therefore, when comparing the two strategies, the data obtained by TCS is an average of 10 simulations.

为了比较两种系统在不同终端区域结构和控制策略下的性能，本文构建了一个实例场景，该场景中的待排序航班量为 $10/20/\ldots/100$ ，并假设 ETA 间隔遵循 $\lambda = 60$ 的泊松分布。进近航班的初始功率呈正态分布，平均值为 35% ，标准差为 5%，而起飞航班的初始功率呈正态分布，平均值为 92%，标准差为 2.5%。ACS 和 TCS 的计算分别基于算法框架 (图 6) 和 ACO。图 11 显示了在航班数量为 20 和 40 的情景中，TCS 的平均航班时间，最大差异分别为 14.82% 和 28.70%。因此，在比较两种策略时，TCS 得到的数据是 10 次模拟的平均值。

Select the operation data with the number of flights to be sorted as 20,50,80,100 respectively for preliminary analysis (In TCS, select the set of flight operation data that is closest to the average). When the number of flights to be sorted is 20 (NumF $= 20$), the slope of flights leaving the terminal area overtime under TCS is slightly greater than that under ACS, i.e. the number of flights leaving the terminal area in unit time under TCS is higher and the operating efficiency is higher (Fig. 12a). With the increase in the number of arrival flights, the number of flights stranded in MVS-TA under TRS increased (i.e., the operation time of each flight increased), the gap between the two control strategies operating efficiency gradually increased, the advantages of ACS became more and more obvious. The maximum gap in the number of stranded terminal flights was 16,23, and 38, respectively, in NumF-50/80/100. (Fig. 12b, 12c, 12d).

选择操作数据，按照 20、50、80、100 个航班的数量分别排序进行初步分析 (在 TCS 中，选择最接近平均值的航班操作数据集)。当排序的航班数量为 20(NumF $= 20$) 时，TCS 下航班离开终端区域随时间变化的斜率略高于 ACS 下的斜率，即 TCS 下单位时间内离开终端区域的航班数量更高，运营效率更高 (图 12a)。随着到达航班数量的增加，TRS 下 MVS-TA 中滞留的航班数量增加 (即每架航班的运营时间增加)，两种控制策略的运营效率差距逐渐增大，ACS 的优势越来越明显。在 NumF-50/80/100 的情况下，滞留终端航班的最大差距分别为 16、23 和 38(图 12b、12c、12d)。

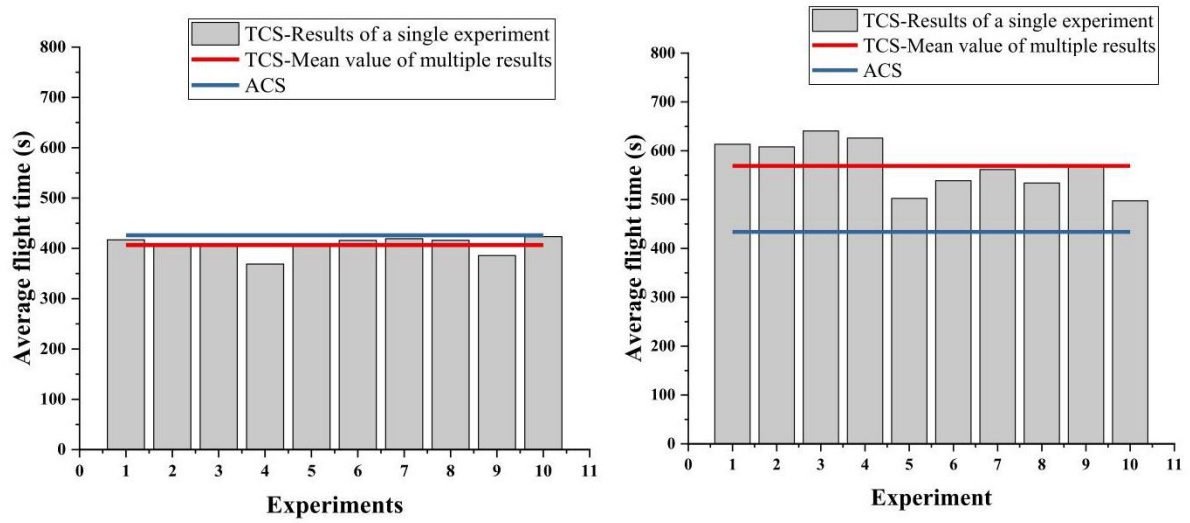

a. Average flight time in MVS-TA in NumF=20 b. Average flight time in MVS-TA in NumF=40

Fig. 11. Multiple result data under TCS in NumF = 20 and NumF = 40 (Note: Average flight time: In the corresponding simulation case, the average flight time of several flights in the terminal area).

图 11。TCS 下 NumF = 20 和 NumF = 40 的多个结果数据 (注: 平均飞行时间: 在相应的模拟案例中，终端区域中几架航班的平均飞行时间)。

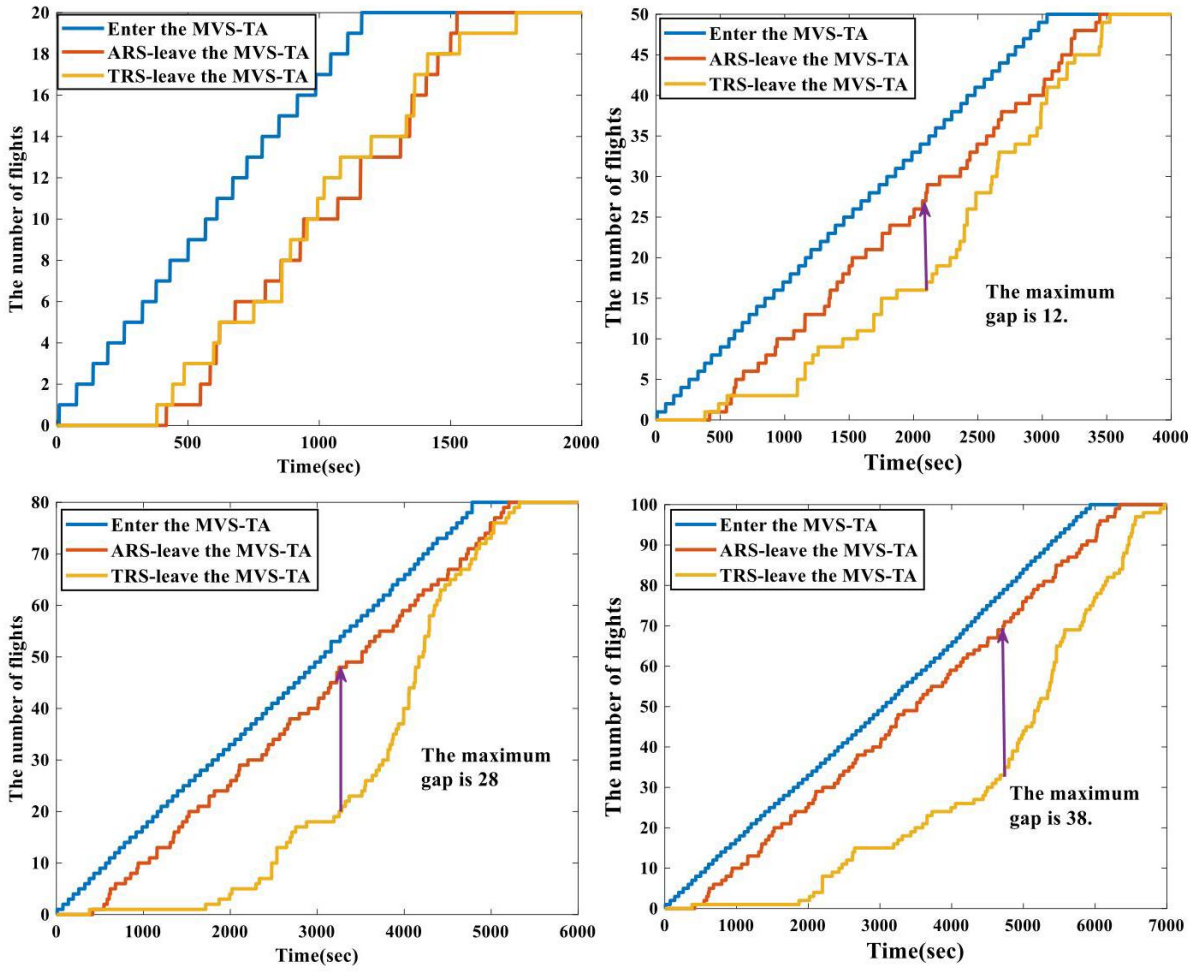

Fig. 12. The cumulative number of flights leaving MVS-TA over time under the ACS and TCS. (a) NumF = 20 ; (b) NumF = 50 ; (c) NumF = 80 ; (c) NumF = 80 ; (d) NumF = 100 .

图 12。在 ACS 和 TCS 下，MVS-TA 随时间累计离开的航班数量。(a)NumF = 20； (b)NumF = 50； (c)NumF = 80； (d)NumF = 100 。

Table 6

表 6

Comparison of flight operation data under ACS and TCS.

ACS 和 TCS 下航班操作数据的比较。

Flights	Average flight time			Standard deviation		Average power consumption			Danger separation		Power alarm	
	ACS	TCS	Gap	ACS	TCS	ACS	TCS	Gap	ACS	TCS	ACS	TCS
10	409.5	406.35	−0.8%	87.1	160.9	0.1107	0.1110	-0.1%	1	0	0	0
20	426	406.58	−4.6%	78.3	100.4	0.1172	0.1093	−6.7%	2	1.2	0	0
30	431.57	473.66	9.8%	76.8	230.8	0.1191	0.1286	8.0%	3	1.1	0	0
40	433.98	568.92	31.1%	73.9	335.6	0.1199	0.1551	29.4%	3	3.3	0	0.3
50	435.9	791.98	81.7%	78.2	552.2	0.1176	0.2154	83.2%	4	6.3	0	1.9
60	436.43	943.74	116.2%	80.3	779.9	0.1189	0.2505	110.7%	4	12.8	0	2.5
70	438.66	1130.08	157.6%	78.7	934.4	0.1161	0.3064	163.9%	4	8.1	0	16.4
80	436.64	1372.89	214.4%	74.8	1141.4	0.1164	0.4041	247.3%	5	11.2	0	23.7
90	439.66	1599.66	263.8%	73.8	1375.1	0.1179	0.4521	283.5%	5	17.2	0	31.1
100	441.08	1845.36	318.4%	77.5	1524.1	0.1164	0.4978	327.7%	7	17.3	0	41.3

航班	平均飞行时间			标准差		平均功率消耗			危险分离		功率警报	
	ACS(空气控制系统)	TCS(牵引力控制系统)	间隙	ACS(空气控制系统)	TCS(牵引力控制系统)	ACS(空气控制系统)	TCS(牵引力控制系统)	间隙	ACS(空气控制系统)	TCS(牵引力控制系统)	ACS(空气控制系统)	TCS(牵引力控制系统)
10	409.5	406.35	−0.8%	87.1	160.9	0.1107	0.1110	-0.1%	1	0	0	0
20	426	406.58	−4.6%	78.3	100.4	0.1172	0.1093	-6.7%	2	1.2	0	0
30	431.57	473.66	9.8%	76.8	230.8	0.1191	0.1286	8.0%	3	1.1	0	0
40	433.98	568.92	31.1%	73.9	335.6	0.1199	0.1551	29.4%	3	3.3	0	0.3
50	435.9	791.98	81.7%	78.2	552.2	0.1176	0.2154	83.2%	4	6.3	0	1.9
60	436.43	943.74	116.2%	80.3	779.9	0.1189	0.2505	110.7%	4	12.8	0	2.5
70	438.66	1130.08	157.6%	78.7	934.4	0.1161	0.3064	163.9%	4	8.1	0	16.4
80	436.64	1372.89	214.4%	74.8	1141.4	0.1164	0.4041	247.3%	5	11.2	0	23.7
90	439.66	1599.66	263.8%	73.8	1375.1	0.1179	0.4521	283.5%	5	17.2	0	31.1
100	441.08	1845.36	318.4%	77.5	1524.1	0.1164	0.4978	327.7%	7	17.3	0	41.3

Note: 1) Average flight time: under the corresponding control strategy, average operation time in MVS-TA for each flight in each case. 2) Average power consumption: under the corresponding control strategy, the average power consumption per flight in the MVS-TA (The remaining electricity of the flight is calculated according to Eq. (28)). 3) Danger separation: when the interval between two flights through the conflict point (conflict port) is less than 20 s (threshold), the alarm is triggered. The statistics in the table are the total number of times the alarm was triggered in the experimental scenario. 4) Power alarm: If the charge of the flight is less than 0 during the operation, the electricity alarm will be triggered. The statistics in the table are the total number of electricity alarms triggered in the simulation.

备注:1) 平均飞行时间: 在相应的控制策略下，MVS-TA 中每次飞行的平均操作时间。2) 平均功耗: 在相应的控制策略下，MVS-TA 中每次飞行的平均功耗 (航班的剩余电量按照公式 (28) 计算)。3) 危险间隔: 当两架航班通过冲突点 (冲突端口) 的时间间隔小于 20 s (阈值) 时，会触发警报。表中的统计数据是在实验场景中触发的警报总次数。4) 功耗警报: 如果在操作过程中航班的电量小于 0，则会触发电力警报。表中的统计数据是在模拟中触发的电力警报总次数。

Further, from the perspective of operational efficiency and safety level, the difference between the two control strategies is explored. The simulation data of each scenario are shown in Table 6.

进一步地，从操作效率和安全性水平的角度，探讨了两种控制策略之间的差异。每个场景的模拟数据如表 6 所示。

Operation efficiency: With the increase in the number of flights to be sorted, the Average flight time of flights under ACS increases slightly (less than7.71%) and stabilized overall, while under TCS there are significant fluctuations. The average operating time of NumF = 10 and NumF = 20 under TCS is 0.8% and 4.6% lower than that of ACS, respectively. The control performance of TCS is slightly better than that of ACS with a low number of flights. The control advantage of ACS is very obvious when the number of flights increases gradually (Fig. 13 a, b). Combined with Fig. 12, when the flight enters the terminal area at intervals of about 60 s, ACS can keep the number of flights staying in MVS-TA stable and low, ensuring the effectiveness and efficiency of scheduling.

操作效率: 随着待排序航班数量的增加，在 ACS 下的航班平均飞行时间略有增加 (小于 7.71%)，总体上保持稳定，而在 TCS 下则有显著波动。TCS 下 NumF = 10 和 NumF = 20 的平均操作时间分别比 ACS 下的低 0.8% 和 4.6% 。在航班数量较少时，TCS 的控制性能略优于 ACS。随着航班数量的逐渐增加，ACS 的控制优势非常明显 (图 13 a, b)。结合图 12，当航班以约 60 秒的间隔进入终端区域时，ACS 可以保持 MVS-TA 中的航班数量稳定且低，确保调度有效性和效率。

Safety level: The average power consumption of the flights in the terminal area is positively related to the Average flight time. The average power consumption of the flights under ACS is 0.11-0.12, which is in a stable and acceptable range. Relatively speaking, when the number of flights to be sorted is 80, the average power

consumption of TCS has reached 0.4041, which is more than 3 times that of ACS, and has exceeded the initial power average (0.35) set by the approach-flight experiment. When the volume of flights to be sorted is further increased to 100, the average power consumption of the flights under TCS is as high as 0.4978, which is about 4.3 times that of ACS. In the experimental scenario of NumF $= 70/80/90/100$, due to the long time of flights under TCS in the terminal area,16.4 (23.4%), 23.7 (29.6%), 31.1 (34.6%) and 41.3 (41.3%) flights respectively ran out of power, triggering the power alarm. This situation is undoubtedly a fatal risk for eVTOL, which uses electricity as the only power source. In addition, this paper puts forward the "Danger separation alarm" as an indicator to compare the two control systems in terms of safety: The distance between the innermost ring layer of the MVS-TA and vertiports is short, and it has the characteristics of small airspace range and complex route structure, which is more likely to produce danger separation than other ring layers. In this paper, the eight points in the innermost layer of the traditional airspace structure are set to the monitoring points of the danger separation alarm. The ten junctions in the innermost layer of the MVS-TA are set to the monitoring points of the alarm. A conflict alarm is triggered when two flights pass through the conflict point (conflict port) for less than the threshold. When the number of flights to be sorted is greater than 40, the number of danger separation alarms under TCS is higher than ACS (Fig. 13c).

安全等级: 终端区域内航班的平均功耗与平均飞行时间呈正相关。在 ACS 控制下的航班平均功耗为 0.11-0.12，处于稳定且可接受的范围内。相对而言，当需要排序的航班数量为 80 时，TCS 的平均功耗已达到 0.4041，是 ACS 的 3 倍以上，并超过了进近实验设定的初始平均功耗 (0.35)。当需要排序的航班数量进一步增加到 100 时，TCS 下的航班平均功耗高达 0.4978，约为 ACS 的 4.3 倍。在 NumF $= 70/80/90/100$ 的实验场景中，由于 TCS 下的航班在终端区域停留时间较长，分别有 16.4(23.4%)、23.7(29.6%)、31.1(34.6%) 和 41.3(41.3%) 的航班耗尽电量，触发了电力警报。这种情况对于仅使用电力作为唯一动力源的 eVTOL 来说无疑是致命的风险。此外，本文提出了“危险分离警报”这一指标，用以比较两种控制系统在安全性方面的差异:MVS-TA 最内层环与垂起降场的距离较近，具有较小的空域范围和复杂的航线结构，比其他环层更易产生危险分离。本文将传统空域结构最内层的八个点设置为危险分离警报的监测点。将 MVS-TA 最内层的十个交接点设置为警报监测点。当两架航班在低于阈值的冲突点 (冲突港口) 通过时，会触发冲突警报。当需要排序的航班数量大于 40 时，TCS 下的危险分离警报数量高于 ACS(见图 13c)。

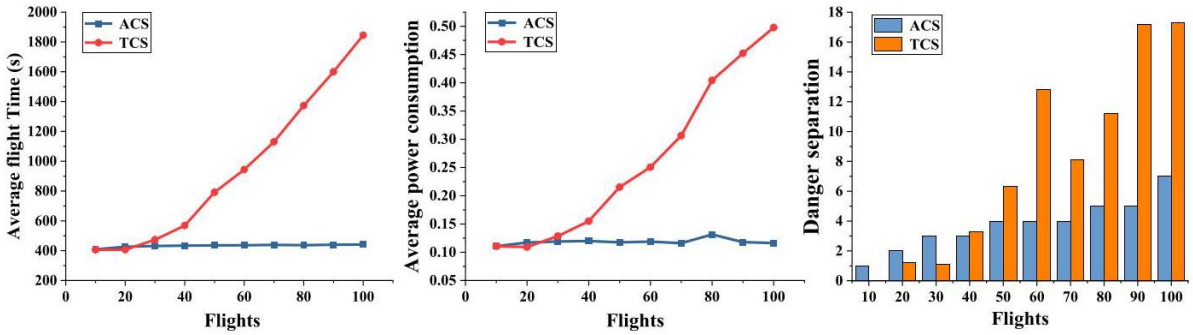

Fig. 13. TCS and ACS performance comparison (a) the average flight time of each flight in the MVS-TA (b) average power consumption (c) the number of danger separation alarms.

图 13. TCS 和 ACS 性能比较 (a)MVS-TA 中每次飞行的平均飞行时间 (b) 平均功耗 (c) 危险间隔警报的数量。

It should be noted that (Vincent et al., 2018) suggests that the DWC (Detect and Avoid Well-Clear) definition of terminal airspace should define vertical intervals of 450ft, HMD (Horizontal Miss Distance) should be 1000ft-2000ft, and τ should be 15sec-25sec. For this reference, this section sets the threshold for danger separation alarm to 20sec.

应该注意的是 (Vincent et al., 2018) 建议，DWC(检测与避让清晰) 对终端空域的定义应设定垂直间隔为 450 英尺，HMD(水平错过距离) 应为 1000 英尺至 2000 英尺，且 τ 应为 15 秒至 25 秒。参照此标准，本节将危险间隔警报的阈值设定为 20 秒。

Due to the limitations of TCS, the number of flights accommodated in the terminal area is lower than the adaptive terminal area structure. When the number of flights increases and cannot land in the vertiport (or leave the terminal area) in time, the operation time will increase. TCS only limits the time separation through the approach-departure fixes, and can not control the other junctions. The increase in the number of flights and flight density will bring an unacceptable risk of danger separation. Relatively speaking, when the ETA intervals are subject to the Poisson distribution of $\lambda = 60$, the performance of ACS is relatively stable, and the average flight time and average power consumption are at a low level.

由于 TCS 的限制，终端区域内可容纳的航班数量低于自适应终端区域结构。当航班数量增加且不能及时在垂直机场着陆 (或离开终端区域) 时，运行时间将会增加。TCS 仅通过进近-起飞固定点限制时间间隔，且无法控制其他交接点。航班数量和飞行密度的增加将带来不可接受的危险间隔风险。相对而言，当 ETA 间隔遵循 $\lambda = 60$ 的泊松分布时，ACS 的性能相对稳定，平均飞行时间和平均功耗都处于较低水平。

It should be noted that although the number of danger separation alarms under ACS also has a slight increase with the increase in flight volume, the design and rules of the concept structure itself greatly reduce the probability that flight danger separation will lead to conflict. Most junctions in the conceptual structure include shadow nodes (flights can only be remitted out of the ring layer, no signal light control) and control nodes (signal control nodes). The structure can guarantee the separation(60s)of the flight through the control node. Because the shadow node of the same intersection is close to the control node, the danger separation alarms can also be triggered if the interval between two flights through the same intersection is less than 20 s . This is the source of most danger separation alarms in ACS and is the main reason why alarms still exist in low flight volume cases. It is worth noting that the flight routes at these two points are different, and the possibility of danger has been greatly reduced.

应该注意的是，尽管随着航班量的增加，在自动冲突分离系统 (ACS) 下的危险分离警报数量也有所轻微增加，但是概念结构本身的设计和规则大大降低了飞行危险分离导致冲突的可能性。概念结构中的大多数节点包括阴影节点 (航班只能从环层发出，没有信号灯控制) 和控制节点 (信号控制节点)。该结构可以通过控制节点保证飞行的分离 (60 秒)。因为相同交叉点的阴影节点靠近控制节点，如果两架航班通过同一交叉点的间隔小于 20 s，也会触发危险分离警报。这是 ACS 中大多数危险分离警报的来源，也是低航班量情况下警报仍然存在的主要原因。值得注意的是，这两点的飞行路线是不同的，危险的可能性已经大大降低。

5.2.2.The impact of flight characteristics on ACS operating performance

5.2.2. 航班特性对 ACS 运行性能的影响

Experiment 1 has proved the efficiency and safety of ACS relative to TCS. ACS guarantees the stability of the flight's running time and power consumption in the terminal area when the ETA intervals are subject to the Poisson distribution of $\lambda = 60$. Experiment 2 will continue to explore the impact of flight volume and flight entry interval (flight density) on the operational performance of ACS.

实验 1 已经证明了 ACS 相对于 TCS 的效率和安全性。当预计到达时间 (ETA) 间隔遵循 $\lambda = 60$ 的泊松分布时，ACS 能够保证终端区域内航班的运行时间和能耗的稳定性。实验 2 将继续探讨航班量和航班进入间隔 (航班密度) 对 ACS 运行性能的影响。

The intervals between the time of flight entering MVS-TA (ETA) are set to obey the Poisson distribution of $\lambda = 60, \lambda = 40, \lambda = 30$, $\lambda = 20$ respectively. For the same ETA interval, different flight volumes are set. The simulation cases are shown in Table 7.

设定航班进入 MVS-TA(ETA) 的时间间隔分别遵循 $\lambda = 60, \lambda = 40, \lambda = 30$ ，$\lambda = 20$ 的泊松分布。对于相同的 ETA 间隔，设置不同的航班量。模拟案例如表 7 所示。

The number of flights stranded in the terminal area at a given time is the difference between the cumulative number of flights entering and leaving the terminal area at that time. When the ETA interval is gradually reduced (the density of flights to be sorted increases), the continuous flight into the terminal area increases the system load, so that the delay time and average running time increase due to the increase of the queue length of the junction. The flight that cannot reach the destination in time will always run in the route network, so the number of flights stranded in the terminal area at every moment is increasing. With the increase in the number of flights, the number of flights stranded in the terminal area at each time in SCE1/SCE2/SCE3 (ETA-interval average is 60 s/ 40 s/30 s) remains volatile and stable, with the upper limit remaining at $10/15/20$, respectively. However, there has been a marked increase in the number of flights stranded at various times in SCE4, which is 1.65 times, 1.95 times, 2.4 times, 2.7 times that of SCE3, respectively (Fig. 14).

在给定时间内，机场终端区域滞留的航班数量是进入和离开该区域累积航班数量的差值。当预计到达时间间隔逐渐减少 (待排序航班密度增加) 时，连续进入终端区域的航班增加了系统负载，导致由于节点队列长度的增加，延迟时间和平均运行时间增加。无法按时到达目的地的航班将在路由网络中持续运行，因此，在每一时刻机场终端区域滞留的航班数量在不断增加。随着航班数量的增加，在 SCE1/SCE2/SCE3(预计到达时间间隔平均为 60 秒/ 40 s/30 s) 中，每个时间点机场终端区域滞留的航班数量保持波动和稳定，上限分别保持在 $10/15/20$ 。然而，在 SCE4 中，各个时间点滞留的航班数量明显增加，分别是 SCE3 的 1.65 倍、1.95 倍、2.4 倍、2.7 倍 (图 14)。

From the point of view of system efficiency: 1) When the average ETA interval of $60\ s/40\ s/30$ s (the density of the flight to be sorted is small) and unchanged, the average flight time increases with the increase in the number of flights, but the fluctuation is small (296-7%). When the average ETA interval is 20 s , the average flight time

increases significantly as the number of flights increases (Fig. 15), and the average hover time (average delay time) is similar to the trend of the Average flight time. 2)When the number of flights is certain, with the increase of the density of flights to be sorted, the average flight time, average delay time and other indicators have also increased (Fig. 15, Table 8), especially in the case of ETA intervals of 20 s and high flight volume. Compared to SCE1 (Baseline), the average flight time of SCE2 and SCE3 in the same flight volume increased by 396-7% and 3%-10%, respectively, while the operational efficiency of the terminal area in SCE4 was greatly reduced. The average operating time increased by 16%-15% in SCE4, and the average delay time in SCE4-3/SCE4-4/SCE4-5 was about 6.7 times, 9.1 times and 10 times the baseline, respectively.

从系统效率的角度来看:1) 当 60 s/40 s/30 s 的平均预计到达时间间隔 (待排序的航班密度较小) 不变时，随着航班数量的增加，平均飞行时间也随之增加，但波动较小 (296-7%)。当平均预计到达时间间隔为 20 s 时，随着航班数量的增加，平均飞行时间显著增加 (见图 15)，平均悬停时间 (平均延误时间) 的变化趋势与平均飞行时间相似。2) 当航班数量确定时，随着待排序航班密度的增加，平均飞行时间、平均延误时间等指标也相应增加 (见图 15、表 8)，特别是在预计到达时间间隔为 20 s 且航班数量大的情况下。与基准 SCE1 相比，相同航班数量下 SCE2 和 SCE3 的平均飞行时间分别增加了 396-7% 和 3%-10%，而 SCE4 的终端区运行效率大幅降低。SCE4 的平均运行时间增加了 16%-15%，SCE4-3/SCE4-4/SCE4-5 的平均延误时间分别是基准的约 6.7 倍、9.1 倍和 10 倍。

Table 7
表 7
Experimental cases.
实验案例。

	Scenario	The number of flights to be sorted (NumF)	ETA interval.	Initial electricity
SCE1	SCE1-1	50	$\lambda = 60$ Poisson	The initial electricity of approaching flights is subject to $N\left(0.35, 0.05^2\right)$
	SCE1-2	100	Distribution	
	SCE1-3	150		
	SCE1-4	200		
	SCE1-5	250		
SCE2	SCE2-1	50	$\lambda = 40$ Poisson	
	SCE2-2	100	Distribution	
	SCE2-3	150		
	SCE2-4	200		
	SCE2-5	250		
SCE3	SCE3-1	50	$\lambda = 30$ Poisson	The initial electricity of departing flights subject to $N\left(0.92, 0.025^2\right)$
	SCE3-2	100	Distribution	
	SCE3-3	150		
	SCE3-4	200		
	SCE3-5	250		
SCE4	SCE4-1	50	$\lambda = 20$ Poisson	
	SCE4-2	100	Distribution	
	SCE4-3	150		
	SCE4-4	200		
	SCE4-5	250		

	场景	需要排序的航班数量 (NumF)	预计到达时间 (ETA) 间隔	初始电力
SCE1	SCE1-1	50	$\lambda = 60$ 泊松	接近航班的初始电力受 $N\left(0.35, 0.05^2\right)$ 的约束
	SCE1-2	100	分布	
	SCE1-3	150		
	SCE1-4	200		
	SCE1-5	250		
SCE2	SCE2-1	50	$\lambda = 40$ 泊松	
	SCE2-2	100	分布	
	SCE2-3	150		
	SCE2-4	200		
	SCE2-5	250		
SCE3	SCE3-1	50	$\lambda = 30$ 泊松	出发航班的初始电力受 $N\left(0.92, 0.025^2\right)$ 影响
	SCE3-2	100	分布	
	SCE3-3	150		
	SCE3-4	200		
	SCE3-5	250		
SCE4	SCE4-1	50	$\lambda = 20$ Poisson	
	SCE4-2	100	分布	
	SCE4-3	150		
	SCE4-4	200		
	SCE4-5	250		

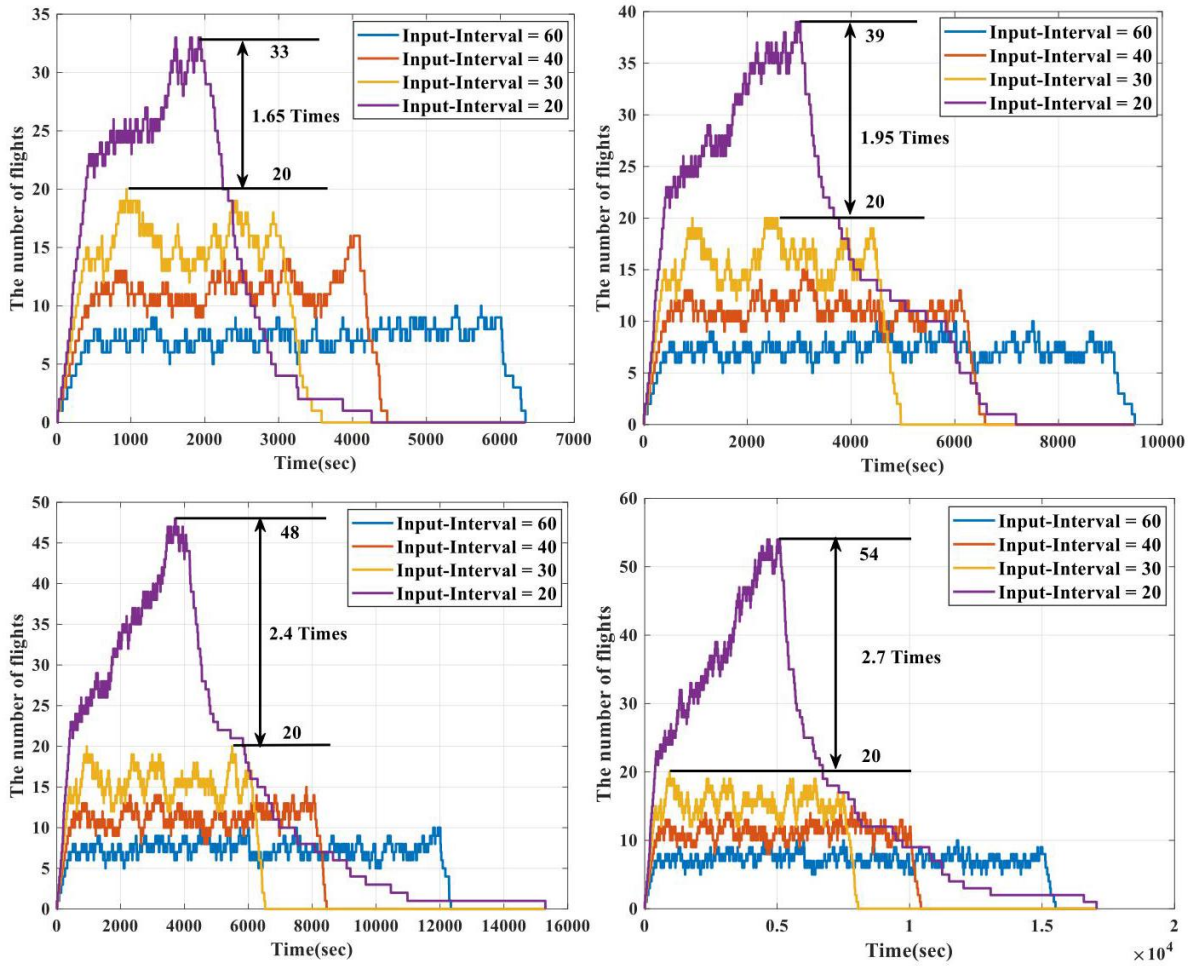

Fig. 14. Number of flights stranded in the terminal area under ACS (a) NumF = 100 (SCE1 − 2/SCE2 − 2/SCE3 − 2/SCE4 − 2
(b) NumF = 150 (SCE1 − 3/) SCE2-3/ SCE3-3/ SCE4-3); (c) NumF = 200 (SCE1-4/ SCE2-4/ SCE3-4/ SCE4-4);
(d) NumF = 250 (SCE1-5/ SCE2-5/ SCE3-5/ SCE4-5).

图 14. 在 ACS 下机场终端区域滞留的航班数量 (a) NumF = 100 (SCE1 − 2/SCE2 − 2/SCE3 − 2/SCE4 − 2)
(b) NumF = 150 (SCE1 − 3/) SCE2-3/ SCE3-3/ SCE4-3); (c) NumF = 200 (SCE1-4/ SCE2-4/ SCE3-4/ SCE4-4);
(d) NumF = 250 (SCE1-5/ SCE2-5/ SCE3-5/ SCE4-5).

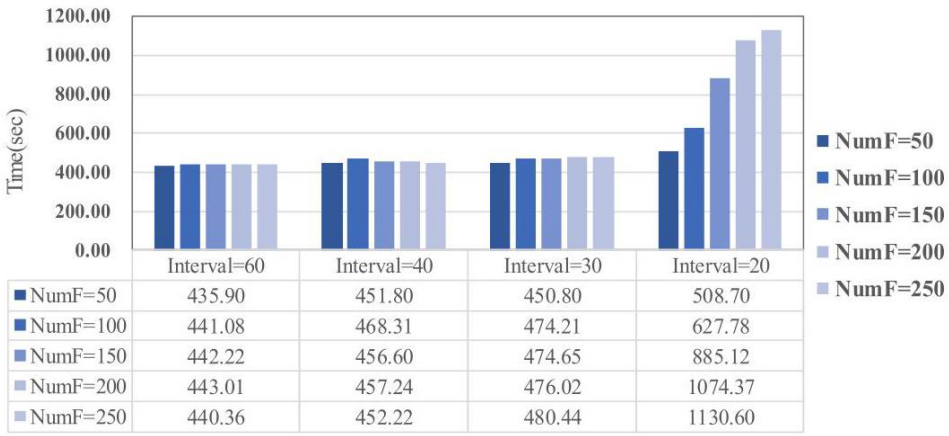

	Interval=60	Interval=40	Interval=30	Interval=20
NumF=50	435.90	451.80	450.80	508.70
NumF=100	441.08	468.31	474.21	627.78
NumF=150	442.22	456.60	474.65	885.12
NumF=200	443.01	457.24	476.02	1074.37
NumF=250	440.36	452.22	480.44	1130.60

Fig. 15. Average flight time in the terminal area.

图 15. 机场终端区域的平均航班时间。

Table 8

表 8
Simulation result data.
模拟结果数据。

Flights		50	100	150	200	250
Average flight time (s)	A = 60 (SCE1)	435.9	441.08	442.22	443.01	440.36
	A = 40 (SCE2)	+3.6%	+6.2%	+3.3%	+3.2%	+2.7%
	A = 30 (SCE3)	+3.4%	+7.5%	+7.3%	+7.5%	+9.1%
	A = 20 (SCE4)	+16.7%	+42.3%	+100.2%	+142.5%	+156.7%
Average power consumption	A = 60 (SCE1)	0.1176	0.1164	0.1186	0.1195	0.1168
	A = 40 (SCE2)	+1.1%	+6.9%	+0.9%	+2.1%	+3.5%
	A = 30 (SCE3)	+1.4%	+10.8%	+7.8%	+8.5%	+11.6%
	A = 20 (SCE4)	+16.4%	+47.3%	+104.6%	+139.7%	+157.7%
Average number of hovers	A = 60 (SCE1)	1.3	1.26	1.17	1.2	1.2
	A = 40 (SCE2)	1.1	1.13	1.15	1.08	1.11
	A = 30 (SCE3)	1.1	1.25	1.21	1.19	1.22
	A = 20 (SCE4)	1.3	1.85	2.35	2.56	2.74
Average hover time (Average delay time) (s)	A = 60 (SCE1)	78.26	79.83	81.04	80.28	78.72
	A = 40 (SCE2)	93.8	109.55	95.13	94.7	90.99
		+19.9%	+37.2%	+17.4%	+18.0%	+15.6%
	A = 30 (SCE3)	94.16	118.75	114.57	113.71	120.93
		+20.3%	+48.8%	+41.4%	+41.6%	+53.6%
	A = 20 (SCE4)	151.66	280.43	538.64	730.86	789.46
		+93.8%	+251.3%	+564.7%	+810.4%	+902.9%
Power alarm	A = 60 (SCE1)	0	0	0	0	0
	A = 40 (SCE2)	0	0	0	0	0
	A = 30 (SCE3)	0	0	0	0	0
	A = 20 (SCE4)	0	1	14	23	30

航班		50	100	150	200	250
平均飞行时间 (秒)	A = 60(SCE1)	435.9	441.08	442.22	443.01	440.36
	A = 40(SCE2)	+3.6%	+6.2%	+3.3%	+3.2%	+2.7%
	A = 30(SCE3)	+3.4%	+7.5%	+7.3%	+7.5%	+9.1%
	A = 20(SCE4)	+16.7%	+42.3%	+100.2%	+142.5%	+156.7%
平均功率消耗	A = 60(SCE1)	0.1176	0.1164	0.1186	0.1195	0.1168
	A = 40(SCE2)	+1.1%	+6.9%	+0.9%	+2.1%	+3.5%
	A = 30(SCE3)	+1.4%	+10.8%	+7.8%	+8.5%	+11.6%
	A = 20(SCE4)	+16.4%	+47.3%	+104.6%	+139.7%	+157.7%
平均悬停次数	A = 60(SCE1)	1.3	1.26	1.17	1.2	1.2
	A = 40(SCE2)	1.1	1.13	1.15	1.08	1.11
	A = 30(SCE3)	1.1	1.25	1.21	1.19	1.22
	A = 20(SCE4)	1.3	1.85	2.35	2.56	2.74
平均悬停时间 (平均延迟时间)(秒)	A = 60(SCE1)	78.26	79.83	81.04	80.28	78.72
	A = 40(SCE2)	93.8	109.55	95.13	94.7	90.99
		+19.9%	+37.2%	+17.4%	+18.0%	+15.6%
	A = 30(SCE3)	94.16	118.75	114.57	113.71	120.93
		+20.3%	+48.8%	+41.4%	+41.6%	+53.6%
	A = 20(SCE4)	151.66	280.43	538.64	730.86	789.46
		+93.8%	+251.3%	+564.7%	+810.4%	+902.9%
功率警报	A = 60(SCE1)	0	0	0	0	0
	A = 40(SCE2)	0	0	0	0	0
	A = 30(SCE3)	0	0	0	0	0
	A = 20(SCE4)	0	1	14	23	30

Note: The percentage of the line of SCE2, SCE3 and SCE4 indicates the gap between the data of this case and that of SCE1.
备注:SCE2、SCE3 和 SCE4 的百分比表示此案例数据与 SCE1 数据之间的差距。

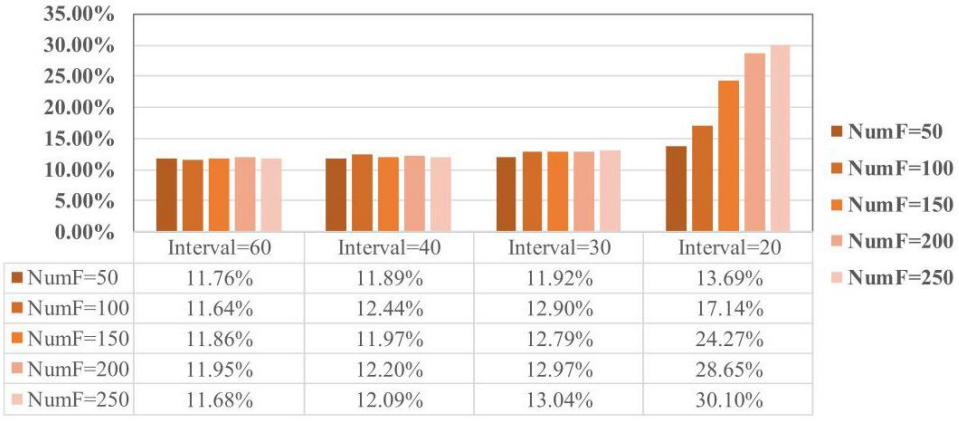

	Interval=60	Interval=40	Interval=30	Interval=20
NumF=50	11.76%	11.89%	11.92%	13.69%
NumF=100	11.64%	12.44%	12.90%	17.14%
NumF=150	11.86%	11.97%	12.79%	24.27%
NumF=200	11.95%	12.20%	12.97%	28.65%
NumF=250	11.68%	12.09%	13.04%	30.10%

Fig. 16. The average power consumption of the flight in the terminal area.
图 16. 机场终端区域航班的平均功耗。

From the point of view of system safety, the average power consumption of the flight in the terminal area is positively related to the average running time. In SCE1/SCE2/SCE3 (ETA interval average is 60 s/40 s/30 s), the average amount of electricity used increases slightly with the number of flights or the density of flights, but no amount of flights is running out of power. In SCE4 (when the ETA interval average is 20 s), the average power consumption of flights increased significantly with the increase in flight volume (Fig. 16), with SCE4-4 and SCE4-5 having 23 (11.5%) and 30 (12%) power alarms, respectively (Table 8). On the one hand, as the number of flights increases, the number of danger separation in SCE1/SCE2/SCE3/SCE4 increases. Since the average ETA interval in SCE4 is 20 s, equal to the conflict threshold(20s), there is a significant increase in the number of dangerous separations in SCE4 (The number of danger separation in NumF = 250 is about 2.89 times higher than that in NumF = 50 , Fig. 17). On the other hand, the number of danger approaches increases with the increase of flight density. As described in 5.2.1, although the number of danger approaches increases with the increase of flight volume, the probability of collision can be greatly reduced because the operation directions of shadow nodes and control nodes are different.

从系统安全的角度来看,终端区域飞行的平均功率消耗与平均运行时间呈正相关。在 SCE1/SCE2/SCE3(预计到达时间间隔平均值是 60 s/40 s/30 s) 中，平均用电量随着航班数量或航班密度的增加略有上升，但没有航班出现电力耗尽的情况。在 SCE4(预计到达时间间隔平均为 20 秒) 中，随着航班量的增加，飞行的平均功率消耗显著增加 (见图 16)，SCE4-4 和 SCE4-5 分别有 23(11.5%) 和 30(12%) 的电力警报 (见表 8)。一方面，随着航班数量的增加，SCE1/SCE2/SCE3/SCE4 中的危险间隔数量增加。由于 SCE4 的平均预计到达时间间隔为 20 秒，等于冲突阈值 (20 秒)，因此在 SCE4 中危险间隔的数量显著增加 (NumF = 250 中的危险间隔数量大约是 NumF = 50 中的 2.89 倍，见图 17)。另一方面，随着航班密度的增加，危险接近的数量也增加。如 5.2.1 节所述，尽管随着航班量的增加，危险接近的数量增加，但由于阴影节点和控制节点的运行方向不同，碰撞的概率可以大大降低。

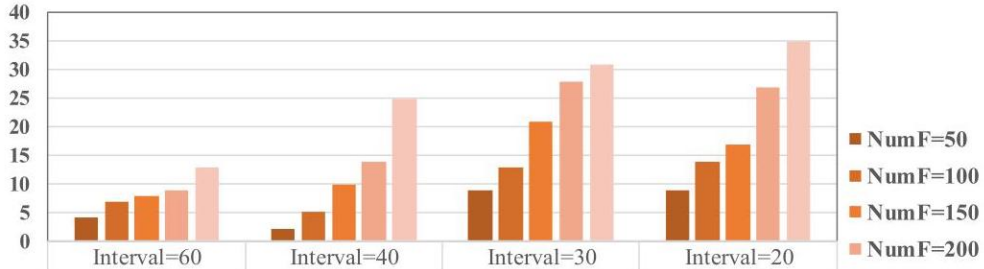

	Interval=60	Interval=40	Interval=30	Interval=20
NumF=50	4	2	9	9
NumF=100	7	5	13	14
NumF=150	8	10	21	17
NumF=200	9	14	28	27
NumF=250	13	25	31	35

Fig. 17. The cumulative number of alarms at the conflicting ports.
图 17. 冲突端口累计警报数量。

5.2.3.ACS performance in random demand scenarios

5.2.3. 随机需求场景下的 ACS 性能

Considering the characteristics of UAM's air transport service in practice, the time of flights entering the terminal area may be random. Experiment 3 sets different number of flights to be sorted during the same period time(1h). The ETA is random, i.e. there may be a situation where a flight of the same/different route enters the terminal area at the same time. The ETA is a random number of [1, 3600]. The average interval of ETA in simulation cases are shown in Table 9. The initial power of the approach flights is subject to the normal distribution $\left(0.35, 0.05^2\right)$, and the initial power of the departure flights is subject to the normal distribution $\left(0.92, 0.025^2\right)$. The number of approach flights is 1.5 times the number of departure flights.

考虑实际中城市空中交通 (UAM) 运输服务的特点，进入终端区域航班的时间可能是随机的。实验 3 在相同时间段内 (1 小时) 设置了不同数量的航班进行排序。预计到达时间 (ETA) 是随机的，即可能存在同一/不同航线的航班同时进入终端区域的情况。预计到达时间是一个 [1, 3600] 范围内的随机数。模拟案例中的预计到达时间平均间隔如表 9 所示。进近航班的初始能量服从 $\left(0.35, 0.05^2\right)$ 的正态分布，而起飞航班的初始能量服从 $\left(0.92, 0.025^2\right)$ 的正态分布。进近航班数量是起飞航班数量的 1.5 倍。

Overall, with the increase in the number of FIM per hour, the average operating time and average delay time of each flight increased relatively small when the flight density was 100/hour and 150/hour. The increase in these two indicators increased significantly as the flight density continued to increase (Fig. 18). When the flight density is 2 times that of the baseline scenario, the average operating time and average power consumption of flights in SCE5-2 increased by less than 7%, and the total scheduled operation time increased by only 3.0% (Table 10). When the flight density is three times that of the baseline scenario, the average flight time and average power consumption in SCE5-3 increased by 12.4% and 12.0%, respectively, and the total operation time increased by less than 5%. There is no alarm of flight power exhaustion in SCE5-1/SCE5-2/SCE5-3. In the SCE5-4 and SCE5-5 scenarios, the flight density into the MVS-TA within 1 h is four and five times that of the baseline scenario, respectively. The average flight time of SCE5-4 and SCE5-5 increased significantly, by 59.3% and 50.7% , respectively, of which the total operation time of SCE5-5 was approximately 1.5 times that of SCE5-1. Besides, 9 aircrafts (4.50%) and 21 aircrafts (8.40%) triggered the power alarm, and the safety level was reduced to a certain extent.

总的来说，随着每小时的航班信息管理 (FIM) 数量的增加，当航班密度为 100/小时和 150/小时时，每架航班的平均运行时间和平均延误时间相对较小地增加。当航班密度继续增加时，这两个指标的增长显著 (见图 18)。当航班密度是基准情景的两倍时，SCE5-2 中的航班的平均运行时间和平均能耗增加不到 7%，总计划运行时间仅增加了 3.0% (表 10)。当航班密度是基准情景的三倍时，SCE5-3 中的航班的平均飞行时间和平均能耗分别增加了 12.4% 和 12.0%，总运行时间增加了不到 5%。在 SCE5-1/SCE5-2/SCE5-3 中没有出现航班能耗耗尽的警报。在 SCE5-4 和 SCE5-5 情景中，进入 MVS-TA 的航班密度分别是基准情景的四倍和五倍。SCE5-4 和 SCE5-5 的平均飞行时间显著增加，分别增加了 59.3% 和 50.7% ，其中 SCE5-5 的总运行时间大约是 SCE5-1 的 1.5 倍。此外，有 9 架飞机 (4.50%) 和 21 架飞机 (8.40%) 触发了能耗警报，安全水平在一定程度上降低。

Table 9

表 9

The average interval of ETA for random demand scenarios.

随机需求场景下预计到达时间 (ETA) 的平均间隔。

Scenario	Frequency	Average interval of ETA (s)
SCE5-1	50 flights/hour	67.20
SCE5-2	100 flights /hour	35.24
SCE5-3	150 flights /hour	23.79
SCE5-4	200 flights /hour	17.81
SCE5-5	250 flights /hour	14.37

场景	频率	预计到达时间 (ETA) 的平均间隔 (秒)
SCE5-1	每小时 50 个航班	67.20
SCE5-2	每小时 100 个航班	35.24
SCE5-3	每小时 150 个航班	23.79
SCE5-4	每小时 200 个航班	17.81
SCE5-5	每小时 250 个航班	14.37

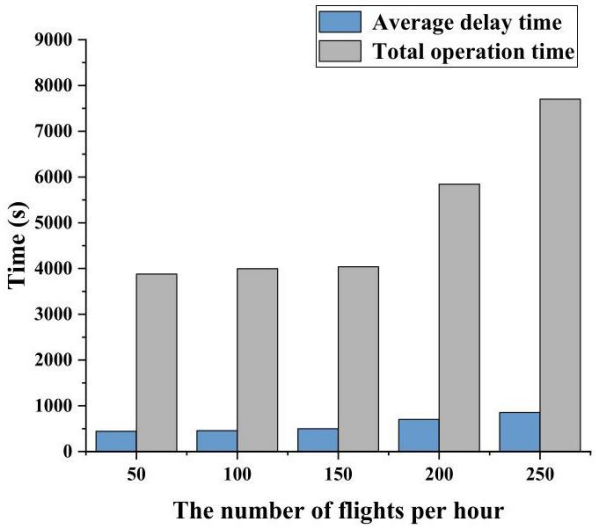

Fig. 18. Average flight time and average delay time for flights in ACS.

图 18。ACS 中航班的平均飞行时间和平均延误时间。

Specifically, as flight density increases, ACS can increase the number of flights that end the terminal operation phase per unit time through effective scheduling (Fig. 19). When the frequency of entry to the MVS-TA is 50/100 (NumF = 50/ hour, NumF = 100/ hour), due to the large average interval of ETAs (67.20 s/35.24 s, respectively, Table 9), the number of flights stranded at each time in the terminal area is not greater than 20 and the operation is stable. When NumF grows to 200 or 250 per hour, the system is unable to schedule flights to the destination in time due to the small intervals between ETAs (17.81 s and 14.37 s , respectively). Therefore, the number of flights stranded in the terminal area always has increased significantly, and in the SCE5-5 scenario the value has reached 67 (Fig. 20) at t = 3067 . This is why the Average flight time, the average power consumption increased greatly, and the operating efficiency and safety level of the MVS-TA decreased significantly.

具体来说，随着航班密度的增加，通过有效的调度 (见图 19)，ACS 可以增加每单位时间内完成终端操作阶段的航班数量。当进入 MVS-TA 的频率为 50/100(NumF = 50/ 小时，NumF = 100/ 小时) 时，由于预计到达时间 (ETA) 的平均间隔较大 (分别为 67.20 秒和 35.24 秒，见表 9)，在终端区每次滞留的航班数量不超过 20 架，运行稳定。当 NumF 增长到每小时 200 或 250 架时，由于 ETA 之间的间隔较小 (分别为 17.81 秒和 14.37 s)，系统无法及时调度航班到达目的地。因此，终端区滞留的航班数量总是显著增加，在 SCE5-5 场景下该值在 t = 3067 时已达到 67(见图 20)。这就是为什么平均飞行时间、平均能耗大幅增加，而 MVS-TA 的运行效率和安全性显著降低的原因。

Table 10

表 10

Results data for ACS in random demand scenarios.

随机需求场景下 ACS 的结果数据。

Case		Average flight time (s)	Average power consumption	Total operation time (s)	Average delay time (s)
SCE5-1	50/hour	443.4	0.1179	3879	86.2
SCE5-2	100/hour	455.35 (+2.7%)	0.1260 (+6.9%)	3995 (+3.0%)	97.06 (+12.6%)
SCE5-3	150/hour	498.17	0.132	4040	140.71
		(+12.4%)	(+12.0%)	(+4.2%)	(+63.2%)
SCE5-4	200/hour	701.56	0.1878%	5845	357.13
		(+58.2%)	(+59.3%)	(+50.7%)	(+314.3%)
SCE5-5	250/hour	853.27	0.2269	7703	515.29
		(+92.4%)	(+92.4%)	(+98.6%)	(+497.8%)
Case		The average TL interval of the system (s)	Average number of hovers	Danger separation	Power alarm
SCE5-1	50/hour	222.32	1.16	3	0
SCE5-2	100/hour	119.79	1.25	11	0
SCE5-3	150/hour	77.15	1.73	19	0
SCE5-4	200/hour	58.07	1.33	23	9(4.50%)
SCE5-5	250/hour	61.04	1.5	41	21(8.40%)

案例		平均飞行时间 (秒)	平均功耗	总运行时间 (秒)	平均延迟时间 (秒)
SCE5-1	50/小时	443.4	0.1179	3879	86.2
SCE5-2	100/小时	455.35 (+2.7%)	0.1260 (+6.9%)	3995 (+3.0%)	97.06 (+12.6%)
SCE5-3	150/小时	498.17	0.132	4040	140.71
		(+12.4%)	(+12.0%)	(+4.2%)	(+63.2%)
SCE5-4	200/小时	701.56	0.1878%	5845	357.13
		(+58.2%)	(+59.3%)	(+50.7%)	(+314.3%)
SCE5-5	250/小时	853.27	0.2269	7703	515.29
		(+92.4%)	(+92.4%)	(+98.6%)	(+497.8%)
案例		系统的平均时间间隔 (秒)	平均悬停次数	危险间隔	功率警报
SCE5-1	50/小时	222.32	1.16	3	0
SCE5-2	100/小时	119.79	1.25	11	0
SCE5-3	150/小时	77.15	1.73	19	0
SCE5-4	200/小时	58.07	1.33	23	9(4.50%)
SCE5-5	250/小时	61.04	1.5	41	21(8.40%)

Note: (1) The percentage of the line of SCE5-2, SCE5-3, SCE5-4 and SCE5-5 indicates the gap between the data of this case and that of SCE5-1. (2) The average TL interval of the system represents the average take-off and landing intervals of the three airports in the system. The smaller the value, the higher the ACS efficiency in the corresponding case.

备注:(1)SCE5-2、SCE5-3、SCE5-4 和 SCE5-5 的百分比表示该案例数据与 SCE5-1 数据之间的差距。(2)系统的平均 TL 间隔代表系统中三个机场的平均起飞和着陆间隔。数值越小，对应案例中 ACS 的效率越高。

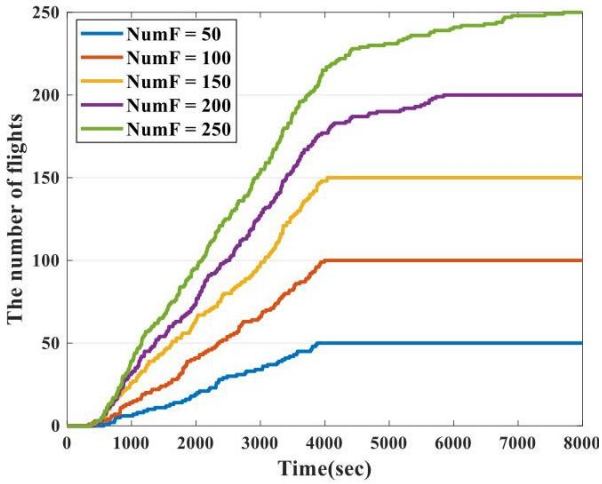

Fig. 19. The cumulative number of flights leaving the terminal area at each time.
图 19. 每个时间点离开终端区的累积航班数量。

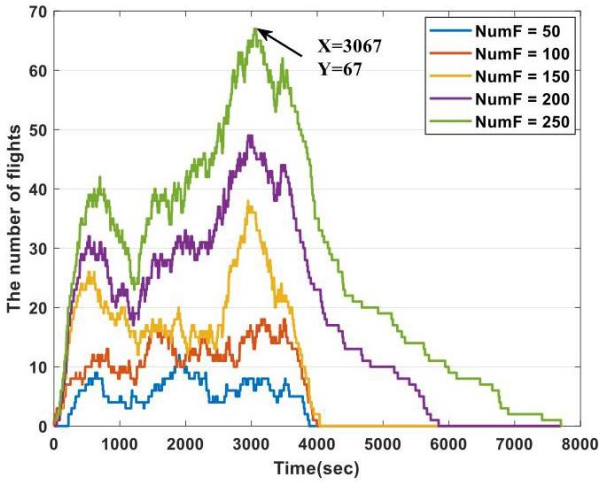

Fig. 20. Number of flights stranded in the terminal area.
图 20. 终端区滞留的航班数量。

6. Conclusion

6. 结论

This paper creatively proposes a set of adaptive control system for MVS-TA, including the concept of multi-ring structure, transit junction control rules, and flight integrated scheduling model. Under the similar terminal area route structure, set up a multi-group experiment with equal flight interval and different flight volume, and compare the ACS with the TCS. In addition, different flight scenarios are set to analyze the main factors affecting ACS.

本文创造性地提出了针对 MVS-TA 的一套自适应控制系统，包括多环结构概念、过渡接点控制规则和飞行综合调度模型。在相似的终端区域航线结构下，建立具有相等航班间隔和不同航班量的多组实验，并将 ACS 与 TCS 进行比较。此外，设置了不同的飞行场景以分析影响 ACS 的主要因素进行分析。

The conclusions can be drawn by ACS compared with TCS: 1) When the average interval between ETAs is at normal levels (60 s) and flight volumes are low (10 or 20), the control performance of TCS is slightly better than that of ACS. As the number of flights increases, ACS's control advantages become more prominent, with the average flight time under TCS already up to 4.2 times that of ACS when NumF is 100.2) When the average flight arrival interval is 60 s , with the increase of flight volume, the average power consumption of flights under ACS remains at 0.11-0.12, no power alarm. The maximum average power consumption under TCS is 0.4978, which is about four times that of TCS, and up to 40% of flights are alarmed. One of the major tasks of UAM is commuter flights. TCS is relatively unable to meet the operational requirements of the peak hours, and ACS is obviously more able to meet the operational efficiency and reliability of UAM.

通过将 ACS 与 TCS 进行比较，可以得出以下结论:1) 当预计到达时间 (ETA) 的平均间隔处于正常水平 (60 秒) 且航班量较低 (10 或 20) 时，TCS 的控制性能略优于 ACS。随着航班数量的增加，ACS 的控制优势变得更加明显，当 NumF 为 100 时，TCS 下的平均飞行时间是 ACS 的 4.2 倍。2) 当平均飞行到达间隔为 60 s 时，随着航班量的增加，ACS 下的平均能耗保持在 0.11-0.12，没有能耗警报。TCS 下的最大平均能耗为 0.4978，大约是 TCS 的四倍，且高达 40% 的航班发出能耗警报。城市空中交通 (UAM) 的主要任务之一是通勤航班。TCS 相对无法满足高峰时段的运营要求，而 ACS 显然更能满足 UAM 的运营效率和可靠性。

Besides, based on the analysis of the experimental data of ACS, the following conclusions can be drawn: 1) Flight arrival density has a greater impact on system recovery efficiency and safety levels than flight volume. When flight density does not meet the system tolerance limit, ACS's operational performance decreases only slightly as the number and density of flights increase (the density $\leq$ 120 flights/hour, the reduction less than 10.3% ; the density $\leq$ 90 flights/hour, the reduction less than 7.5%). ACS can carry out flight scheduling and optimization through effective operation structure and strategy, so that MVS-TA can maintain high efficiency and safety. 2) In the case of random flight entry, ACS can guarantee operational efficiency and safety level stability at flight density of fewer than 150 flights/hour. With the increase of flight density, the time of flight stranded in the terminal area gradually increases, and the operational efficiency decreases. The ACS proposed provides a kind of airspace design for the future development stage of UAM, which can ensure the stability, adaptability, safety, and efficiency of MVS-TA operation.

此外，基于对 ACS 实验数据的分析，可以得出以下结论:1) 飞行到达密度对系统恢复效率和安全性水平的影响大于飞行量。当飞行密度未达到系统容忍极限时，随着航班数量和密度的增加，ACS 的运行性能仅略微下降 (密度 $\leq$ 120 次/小时，下降小于 10.3% ；密度 $\leq$ 90 次/小时，下降小于 7.5%)。ACS 可以通过有效的运行结构和策略进行航班调度和优化，从而使 MVS-TA 保持高效率和安全性。2) 在随机航班进入的情况下，ACS 可以保证在每小时少于 150 架次的飞行密度下，运行效率和安全性水平保持稳定。随着飞行密度的增加，终端区滞留的航班时间逐渐增加，运行效率降低。本文提出的 ACS 为 UAM 未来发展阶段提供了一种空域设计方案，可以确保 MVS-TA 运行的稳定性、适应性、安全性和效率。

The complete adaptive control system proposed in this paper can provide an important reference for the structural design and flight scheduling of MVS-TA in UAM. At the same time, the transit intersection control rules and the integrated scheduling model based on a dynamic route network can also be applied to the control scheduling of UAM urban airspace routes. The futuure research direction is to study the route structure and control rules of UAM in-depth and explore the influence of many factors on operational efficiency and safety performance. Also, explore the uncertainty factors of scheduling optimization to improve the robustness of the model application.

本文提出的完整自适应控制系统为 UAM 中 MVS-TA 的结构设计和飞行调度提供了重要参考。同时，基于动态路由网络的过渡交叉控制规则和集成调度模型也可应用于 UAM 城市空域路由的控制调度。未

来的研究方向是深入研究 UAM 的路由结构和控制规则，探讨多种因素对运行效率和安全性性能的影响，以及探索调度优化中的不确定性因素，以提高模型应用的鲁棒性。

The simulation code for ACS is available at "https://github.com/Amelia55/Adaptive-Control-System-for-UAM".

ACS 的模拟代码可在"https://github.com/Amelia55/Adaptive-Control-System-for-UAM" 获取。

Declaration of Competing Interest

利益冲突声明

The authors declare that they have no known competing financial interests or personal relationships that could have appeared to influence the work reported in this paper.

作者声明，他们没有已知的经济利益冲突或个人关系，这些可能影响到本文报告的工作。

Acknowledgement

致谢

This is work was supported by the National Key R&D Program of China (grant no. 2018YFC0809500), the National Natural Science Foundation of China (grant no. 71874081), and Qing Lan Project of Jiangsu Province of China: 2020.

本工作得到了中国国家级重点研发计划的支持 (项目编号:2018YFC0809500)，中国国家自然科学基金的支持 (项目编号:71874081)，以及中国江苏省的青蓝工程项目:2020 的支持。

References

参考文献

Bertram, J., Wei, P., 2020. An Efficient Algorithm for Self-Organized Terminal Arrival in Urban Air Mobility 1-10. Doi: 10.2514/6.2020-0660.

Bosson, C.S., Lauderdale, T.A., 2018. Simulation evaluations of an autonomous urban air mobility network management and separation service, in: 2018 Aviation Technology, Integration, and Operations Conference. Doi: 10.2514/6.2018-3365.

Brittain, M., Wei, P., 2018. Autonomous Aircraft Sequencing and Separation with Hierarchical Deep Reinforcement Learning. Icrat.

Cotton, W.B., 2019. Adaptive autonomous separation for UAM in mixed airspace. Integr. Commun. Navig. Surveill. Conf. ICNS 2019-April, 1-11. Doi: 10.1109/ ICNSURV.2019.8735119.

Cui, M., 2013. Research on Method of Real-time Travel Time Collection Based on Simplified Road Network Model. Chongqing University.

Duan, H., 2005. Ant Colony Algorithms: Theory and Applications, Science Press.

EHANG216, n.d. EHANG216 Autonomous Aerial Vehicle Specs.pdf [WWW Document]. URL https://www.ehang.com/cn/ehan

Federal Aviation Administration, 2016. Wake Turbulence Recategorization [WWW Document]. URL https://www.faa.gov/docun 7110_123_(2).pdf.

German, B.J., Daskilewicz, M.J., Hamilton, T.K., Warren, M.M., 2018. Cargo delivery by passenger eVTOL aircraft: A case study in the san francisco bay area. AIAA Aerospace Sciences Meeting 2018, 1-13. https://doi.org/10.2514/6.2018-2006.

Hao, E., 2017. Research on Rerouting Tactics in Terminal Area Based on Task Complexity of ATC. Nanjing University of Aeronautics and Astronautics. Syst. 17 (3), 150-159. https://doi.org/10.2514/1.I010776.

Kleinbekman, I.C., Mitici, M.A., Wei, P., 2018. eVTOL arrival sequencing and scheduling for on-demand urban air mobility. AIAA/IEEE Digit. Avion. Syst. Conf. - Proc. 2018-Septe, 1-7. Doi: 10.1109/DASC.2018.8569645.

Le, T., Kovács, P., Walton, N., Vu, H.L., Andrew, L.L.H., Hoogendoorn, S.S.P., 2015. Decentralized signal control for urban road networks. Transp. Res. Part C Emerg. Technol. 58, 431-450. https://doi.org/10.1016/j.trc.2014.11.009.

Li, C., Qu, W., Li, Y., Huang, L., Wei, P., 2020. Overview on traffic management of urban air mobility(UAM) with eVTOL aircraft. J. Traffic Transp. Eng. 20.

Littell, J.D., 2019. Challenges in vehicle safety and occupant protection for autonomous electric vertical take-off and landing (Evtol) vehicles. AIAA Propuls. Energy Forum Expo. 2019 https://doi.org/10.2514/6.2019-4504.

Luo, Y., Zhu, T., Wan, S., Zhang, S., Li, K., 2016. Optimal charging scheduling for large-scale EU (electric vehicle) deployment based on the interaction of the smart-grid and intelligent-transport systems. Energy 97, 359-368. https://doi.org/10.1016/j.energy.2015.12.140.

Ma, D., Xiao, J., Ma, X., 2020. A decentralized model predictive traffic signal control method with fixed phase sequence for urban networks. J. Intell. Transp. Syst Technol. Planning, Oper. 25 (5), 455-468. https://doi.org/10.1080/15472450.202

Mohamed Salleh, M.F. Bin, Tan, D.Y., Koh, C.H., Low, K.H., 2017. Preliminary concept of operations (ConOps) for traffic management of unmanned aircraft systems (TM-UAS) in urban environment, in: AIAA Information Systems-AIAA Infotech @ Aerospace. p. 0223. Doi: 10.2514/6.2017-0223.

4ohammed Salleh, M.F. Bin, Chi, W., Wang, Z., Huang, S., Tan, D.Y., Huang, T., Low, K.H., 2018. Preliminary concept of adaptive urban airspace management for unmanned aircraft operations, in: AIAA Information Systems-AIAA Infotech @ Aerospace. p. 2260. Doi: 10.2514/6.2018-2260.

Pradeep, P., 2019. Arrival Management for eVTOL Aircraft in On-Demand Urban Air Mobility. Grad. Theses Diss.

Pradeep, P., Wei, P., 2018. Energy efficient arrival with rta constraint for urban evtol operations. AIAA Aerrosp. Sci. Meet. 2018, 1-13. https://doi.org/10.2514/ 6.2018-2008.

Prevot, T., Rios, J., Kopardekar, P., Robinson III, J.E., Johnson, M., Jung, J., 2016. UAS Traffic Management (UTM) Concept of Operations to Safely Enable Low Altitude Flight Operations. Doi: 10.2514/6.2016-3292.

Shao, Q., Shao, M., Bin, Y., Zhu, P., Zhou, Y., 2020. Flight Recovery Method of Regional Multiairport Based on Risk Control Model. Math. Probl. Eng. 2020, 1-18. https://doi.org/10.1155/2020/7105381.

Sunil, E., Hoekstra, J., Ellerbroek, J., Bussink, F., Vidosavljevic, A., Delahaye, D., Aalmoes, R., 2016. The Influence of Traffic Structure on Airspace Capacity. Proc. 74h Int. Conf. Res. Air Transp.

Sun, Q., 2020. Research on airspace capacity assessment for airport terminal area. Civil Aviation University of China.

Tassiulas, L., Ephremides, A., 1992. Stability Properties of Constrained Queueing Systems and Scheduling Policies for Maximum Throughput in Multihop Radio

Networks. IEEE Trans. Automat. Contr. 37, 1936-1948. https://doi.org/10.1109/9.182479.

Thipphavong, D.P., Apaza, R.D., Barmore, B.E., Battiste, V., Belcastro, C.M., Burian, B.K., Dao, Q. V., Feary, M.S., Go, S., Goodrich, K.H., Homola, J.R., Jdris, H.R., Kopardekar, P.H., Lachter, J.B., Neogi, N.A., Ng, H.K., Oseguera-Lohr, R.M., Patterson, M.D., Verma, S.A., 2018. Urban air mobility airspace integration concepts and considerations, in: 2018 Aviation Technology, Integration, and Operations Conference. Doi: 10.2514/6.2018-3676.

Varaiya, P., 2013a. The Max-Pressure Controller for Arbitrary Networks of Signalized Intersections. Adv. Dynam. Netw. Model. Complex Transport. Syst. 163–192. https://doi.org/10.1007/978-1-4614-6243-9.

Varaiya, P., 2013b. Max pressure control of a network of signalized intersections. Transp. Res. Part C Emerg. Technol. 36, 1777-195. https://doi.org/10.1016/j.trc.2013.08.014.

Vascik, P.D., Hansman, R.J., 2018. Scaling constraints for urban air mobility operations: Air traffic control, ground infrastructure, and noise. 2018 Aviat. Technol. Integr. Oper. Conf. 1-25 https://doi.org/10.2514/6.2018-3849.

Vidosavljevic, A., Delahaye, D., Sunil, E., Bussink, F., Hoekstra, J., 2015. Complexity Analysis of the Concepts of Urban Airspace Design for METROPOLIS Project. EIWAC 2015, 4th ENRI Int. Work. ATM/CNS.

Vincent, M.J., Trujillo, A.C., Jack, D.P., Hoffler, K., Tsakpinis, D., 2018. A recommended daa well-clear definition for the terminal environment. 2018 Aviat. Technol. Integr. Oper. Conf. https://doi.org/10.2514/6.2018-2873.

Wang, S., Huang, W., Lu, Z., 2006. Deduction of link performance function and its regression analysis. J. Highw. Transp. Res. Dev. 23, 107-110.

Wang, Y., Wang, Q., Wang, H., Jin, H., Dai, G., 2004. A Real-Time Scheduling Algorithm Based on Priority Table and Its Implementation. J. Sofw. 15, 358–368.

Wen, X., Huo, J., 2020. Research Based on Dynamic Priority for a Multi-runway Mixed Arrival-Departure Aircraft Scheduling Problem. Ind. Eng. Manag. 1-15.

Wongpiromsarn, T., Uthaicharoenpong, T., Wang, Y., Frazzoli, E., Wang, D., 2012. Distributed traffic signal control for maximum network throughput. IEEE Conf. Intell. Transp. Syst. Proceedings, ITSC 588-595. Doi: 10.1109/ITSC.2012.6338817.

Wu, Y., Sun, L., Qu, X., 2016. A sequencing model for a team of aircraft landing on the carrier. Aerosp. Sci. Technol. 54, 72–87. https://doi.org/10.1016/j.ast.2016.04.007.

Xu, Y., Zhang, H., Yang, L., Liao, Z., 2015. Analysis of Air Traffic Flow Characteristics in Airport Terminal Area Based on Observed Data. J. Transport. Syst. Eng. Inf. Technol. 15 (1), 205-211. https://doi.org/10.16097/j.cnki.1009-6744.2015.01.032.

Yang, X., Deng, L., Wei, P., 2019. Multi-Agent Autonomous On-Demand Free Flight Operations in Urban Air Mobility 1–13. Doi: 10.2514/6.2019-3520.

Zhang, J., Yang, W., 2018. The Optimization Based on Priority for a Mixed Arrival-Departure Aircraft Sequencing Problem. Oper. Res. Manag. Sci. 27, 115-121. Zhang, J.F., Ge, T.T., Zheng, Z.X., 2017. Collaborative Arrival and Departure Sequencing for Multi-airport Terminal Area. Jiaotong Yunshu Xitong Gongcheng Yu Xinxi/Journal Transp. Syst. Eng. Inf. Technol. 17, 197-204. https://doi.org/10.16097/j.cnki.1009-6744.2017.02.029.

Zhu, G., Wei, P., 2019. Pre-Departure Planning for Urban Air Mobility Flights with Dynamic Airspace Reservation. Doi: 10.2514/6.2019-3519.